BOLU ABANT IZZET BAYSAL UNIVERSITY

THE GRADUATE SCHOOL OF NATURAL AND APPLIED SCIENCES

FABRICATION AND CHARACTERIZATION OF DOPED METAL-OXIDE SEMICONDUCTOR THIN FILM GAS SENSORS

MASTER OF SCIENCE

SİNAN ÖZTEL

BOLU, JULY 2019

BOLU ABANT IZZET BAYSAL UNIVERSITY

THE GRADUATE SCHOOL OF NATURAL AND APPLIED SCIENCES

DEPARTMENT OF PHYSICS

FABRICATION AND CHARACTERIZATION OF DOPED METAL-OXIDE SEMICONDUCTOR THIN FILM GAS SENSORS

MASTER OF SCIENCE

SİNAN ÖZTEL

BOLU, JULY 2019

APPROVAL OF THE THESIS

FABRICATION AND CHARACTERIZATION OF DOPED METAL-OXIDE SEMICONDUCTOR THIN FILM GAS SENSORS submitted by **SİNAN ÖZTEL** and defended before the below named jury in partial fulfillment of the requirements for the degree of **Master of Science** in **Department of Physics, The Graduate School of Natural and Applied Sciences of Bolu Abant İzzet Baysal University in 16.07.2019** by

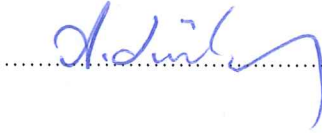**Examining Committee Members**   **Signature**

Supervisor
Prof. Dr. Ercan YILMAZ
Bolu Abant İzzet Baysal University   ....

Member
Assist. Prof. Dr. Erhan BUDAK
Bolu Abant İzzet Baysal University   ....

Member
Assoc. Prof. Dr. Ayşegül KAHRAMAN
Bursa Uludağ University   ....

Prof. Dr. Ömer ÖZYURT   ....

Director of Graduate School of Natural and Applied Sciences
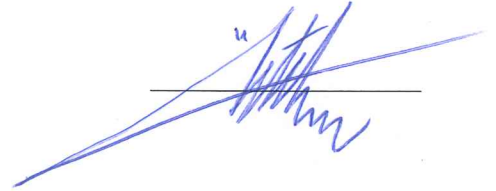
To my family

DECLARATION

I hereby declare that all information in this document has been obtained and presented in accordance with academic rules and ethical conduct. I also declare that, as required by these rules and conduct, I have fully cited and referenced all material and results that are not original to this work.

Sinan ÖZTEL

ABSTRACT

FABRICATION AND CHARACTERIZATION OF DOPED METAL-OXIDE SEMICONDUCTOR THIN FILM GAS SENSORS
MSC THESIS
SİNAN ÖZTEL
BOLU ABANT IZZET BAYSAL UNIVERSITY GRADUATE SCHOOL OF NATURAL AND APPLIED SCIENCES
DEPARTMENT OF PHYSICS
(SUPERVISOR: PROF. DR. ERCAN YILMAZ)

BOLU, JULY 2019

Tin-oxide based thin film gas sensors were produced by Electron Beam Evaporation (e-beam) method and annealed at 600°C. The structural, morphological, chemical and the electrical properties of SnO_2/SiO_2 thin films were studied in detail. The structural analysis were obtained by X-Ray Diffraction (XRD) and Scanning Electron Microscopy (SEM) was used for analyzing the morphological properties of the thin film. Also chemical bonding structures were analyzed via Fourier Transform Infrared Spectroscopy (FTIR) and electrical properties of the SnO_2/SiO_2 thin films were investigated by using current-voltage (I-V) characteristics measurement. Then, by using sputtering technique the Platinum (Pt) was doped onto the produced thin film in 1 second, 3seconds, and 5 seconds respectively. The same structural, morphological, chemical, and the electrical properties of the Pt doped thin films were investigated and discussed. Finally, the Oxygen sensing property of the each fabricated SnO_2/SiO_2 thin films and the effect of Pt doping on gas sensitivity were investigated and discussed in this study.

ÖZET

KATKILI METAL OKSİT YARIİLETKEN İNCE FİLM GAZ SENSÖRLERİNİN ÜRETİMİ VE KARAKTERİZASYONU
YÜKSEK LİSANS TEZİ
SİNAN ÖZTEL
BOLU ABANT İZZET BAYSAL ÜNİVERSİTESİ
FEN BİLİMLERİ ENSTİTÜSÜ
FİZİK ANABİLİM DALI
(TEZ DANIŞMANI: PROF. DR. ERCAN YILMAZ)

BOLU, TEMMUZ - 2019

Kalay oksit bazlı ince film gaz sensörleri Elektron Demeti Buharlaştırma (e-beam) yöntemi ile üretildi ve 600^oC de tavlandı. SnO_2/SiO_2 ince filmlerin yapısal, morfolojik, kimyasal ve elektriksel özellikleri detaylı bir şekilde çalışıldı. Yapısal analizler X-Işını Kırınımı (XRD) ile elde edildi ve ince filmlerin morfolojik özellikleri Taramalı Elektron Mikroskobu (SEM) ile analiz edildi. Ayrıca SnO_2/SiO_2 ince filmlerin kimyasal bağ yapıları Fourier Dönüşüm Kızıl Ötesi Spektroskopi (FTIR) üzerinden analiz edildi ve elektriksel özellikleri akım-voltaj (I-V) karakteristiği kullanılarak araştırıldı. Daha sonrasında üretilen ince filmlere sırasıyla 1 saniye, 3 saniye ve 5 saniye Platin (Pt) kopartma (sputtering) yöntemi ile katkılandı. Pt katkılanmış ince filmlerin aynı şekilde yapısal, morfolojik, kimyasal ve elektriksel özellikleri araştırıldı ve tartışıldı. Son olarak, bu çalışmada üretilen tüm SnO_2/SiO_2 ince filmlerin oksijen algılama özelliği ve Pt katkılanmasının gaz duyarlılığına etkisi araştırıldı ve tartışıldı.

ANAHTAR KELİMELER: İnce Film, Gaz Sensörleri, Oksijen Sensörü, Metaloksit Yarıiletkenler, Kalay Oksit (SnO_2)

TABLE OF CONTENTS

LIST OF FIGURES

LIST OF TABLES

LIST OF ABBREVIATIONS AND SYMBOLS

BAIBU   **:** Bolu Abant İzzet Baysal University

EDS   **:** Energy Dispersive Spectroscopy

FTIR   **:** Fourier Transform Infrared Spectroscopy

FWHM   **:** Full Width at Half Maximum

GUNAM   **:** Center for Solar Energy Research and Applications

I-V   **:** Current-Voltage

ICDD   **:** International Center for Diffraction Data

LASER   **:** Light Amplification by Stimulated Emission of Radiation

NRDC   **:** Nuclear Radiation Detector Research and Application Center

Pa   **:** Pascal

ppm   **:** Parts per Million

RCA   **:** Radio Corporation America

SEM   **:** Scanning Electron Microscopy

XRD   **:** X-Ray Diffraction

ACKNOWLEDGEMENTS

1. INTRODUCTION

It is known that adsorption or desorption of gas molecules on the surface of the metal-oxide materials effects the conductivity. This phenomena was firstly discovered by Seiyama and his friends in 1962 (Cakir, 2014). A lot of pure and semiconducting metal-oxides are used for producing a gas sensor. Tin-oxide based gas sensors are widely used sensors because of their special sensing properties (Zhang and Liu, 2000).

1.1 Gas Sensors and Their Role in Industry, Agriculture, and Environment Control

There are various types of gases inside the atmosphere. Some of the gases are vital for livings but many others are harmful. The concentration of any gas must be under controlled in living atmosphere. For example, gas concentration of O_2 must between 80 ppm and 105 ppm in living atmosphere. Same like O_2 under controlled humidity is also important for the livings. The gas sensor industry is emerging day by day. In Japan, there is houses which have under controlled gas concentration, humidity, and CO_2. Air cleaners with air-quality sensor are using for safety in some facilities. Because, combustive gases must be at fairly low levels (Korotchenkov, 2013, Chapter 1).

More than 30 years gas sensors market became developed in some fields such as oxygen sensing for combustion in exhaust control, monitoring the combustive gas, and humidity sensing. Combustive gas monitoring was first started with semiconductor gas sensors. But, catalytic combustion type of sensors became popular in Europe (Yamazoe, 2005).

It is known that adsorption of gas molecules into a metal-oxide material effects the conductivity of the material since 1962. This phenomenon showed by Seiyama and his friends at the first time. The study showed that zinc oxide (ZnO_2)

was sensitive to reactive gases in the air. Similar studies were performed with tin-oxide (SnO2) and positive results were obtained. Metal-oxide sensors which are simple, low production cost, and proper to mass production were possible thanks to developing of the silicon technology, and micro fabrication technology was developed. Owing to these technologies size of sensors was get smaller and power consumption was also decreased. So, these metal oxide sensors can be used in portable devices (Cakir, 2014).

1.2   Metal-Semiconductor Contacts

The metal-semiconductor contacts have non-linear, rectifying voltage characteristics. These kind of contacts can be named as Schottky contact. This section consists of electrical characteristics of the Schottky contacts.

1.2.1   Schottky Diode

A Schottky diode or as it mentioned before, Schottky contact can be formed as rectifying contact which is formed between semiconductor and a metal. This rectifying property of metal-semiconductor contacts was first discovered bu F. Braun in 1874 and clearly explained by Mott and Schottky in 1938 (Coligne JP and Coligne CA, 2002, Chapter 5).

1.2.2   Energy Band Diagram of Schottky Contacts

As it seen before a Schottky contacts are formed with a metal and a semiconductor. The used semiconductor must be N-Type semiconductor Figure 1.1 shows the energy band diagram of each metal and semiconductor. When a light is in a certain wavelength is used as incident beam onto a material electrons can be extracted from the surface of the material in vacuum. This situation explained by Albert Einstein in photoelectric effect in 1921 (Coligne JP and Coligne CA, 2002, Chapter 5).

The incident beam must have enough energy to electrons get extracted. This energy of incident beam ($E=h\nu$) has to be equal to the work function of the metal ($q\phi_m$) or higher (Coligne JP and Coligne CA, 2002, Chapter 5).

The work function of metal can be described as the necessary energy between the fermi level of metal (E_{Fm}) and vacuum energy level. Same like metals, Semiconductors have required energy for electrons get to be extracted. This energy is equal or higher to ($q\phi_{SC}$). Note that the extracted electrons located on the Fermi level of the semiconductor E_{Fsc} (Coligne JP and Coligne CA, 2002, Chapter 5).
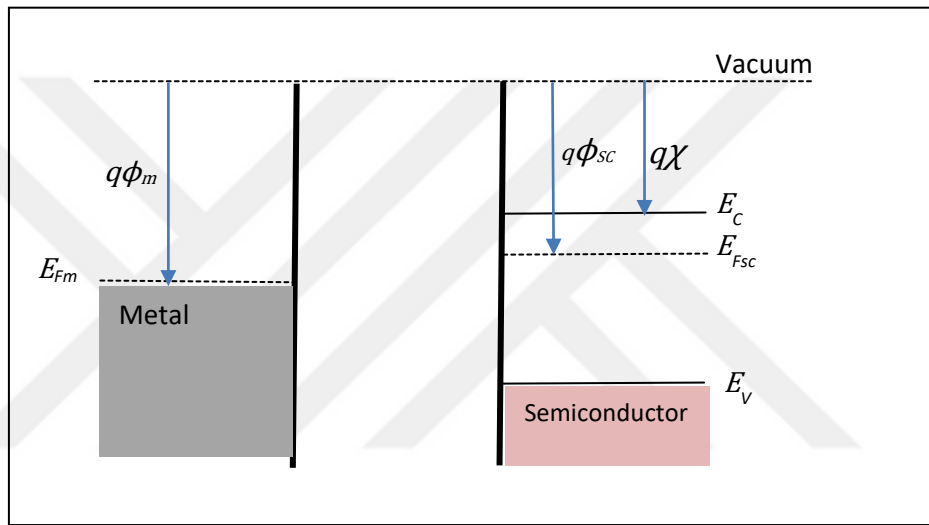
Figure 1.1. Energy band diagram of metal and semiconductor.

Semiconductors have electrons which have energy higher than E_{Fsc} . These electrons are located on the conduction band of the semiconductor. Thiis energy level can be described as E_C. The required energy in order to extract an electron from E_c to vacuum can be called as " electron affinity" and can be note by $q\chi$. In metal-semiconductor contacts we will consider $E_{Fm} < E_{Fsc}$ (Coligne JP and Coligne CA, 2002, Chapter 5).

While the metal-semiconductor contact is formed, the Fermi levels of each materials are lined up and thermodynamic equilibrium is formed electrons start to move from conduction band of semiconductor to metal because energy level of conduction band of semiconductor is higher than the Fermi energy level of the metal. The moved electrons leave a hole behind in the semiconductor. The depleted

3

electrons get into the near to the metal and causes forming of a depletion region W_0 in semiconductor. Then the band curvature of the semiconductor is shown in Eq. (1.1).

$$qV_i = q(\phi_m - \phi_{sc}) \tag{1.1}$$

This potential barrier ϕ_b allows more electrons to get migrate into the metal. So, this barrier named as Schottky barrier (Coligne JP and Coligne CA, 2002, Chapter 5).
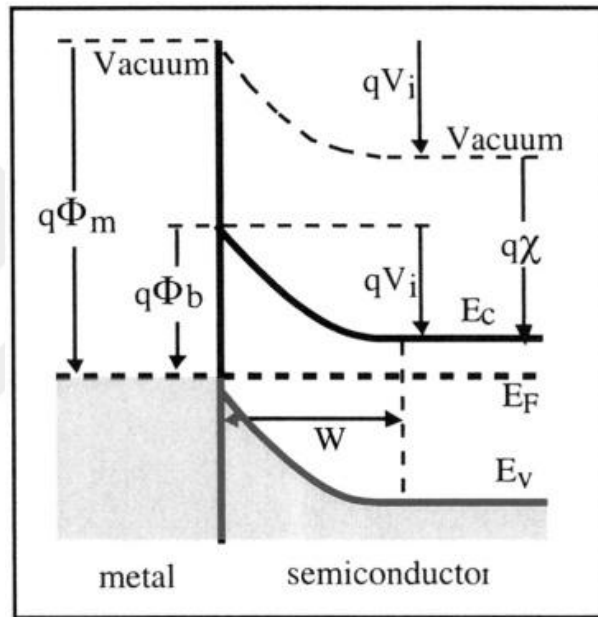
Figure 1.2. Energy band diagram of Schottky contact (Colinge JP and Colinge CA, 2002, p.141).

Then the Schottky barrier can be written in the Eq. (1.2), Schottky barrier is equal to difference between the work finction of the metal and the electron affinity.

$$q\phi_b = q(\phi_m - \chi) = qV_i + (E_c + E_F) \tag{1.2}$$

These potential barriers are larger than kT/q at room temperature. $I_{m \to s}$ represents the movement of electrons from semiconductor to the metal. This movement corresponds a positive current that flows from metal to the semiconductor (Coligne JP and Coligne CA, 2002, Chapter 5).

When the Schottky diode forward biased or positive potential applied, the potential barrier decreases in semiconductor side. So, a lot of electrons migrate from semiconductor to metal and the Schottky barrier does not changes.

In addition when diode reverse biased, the potential barrier increases in semiconductor side. That is why a small amount of current will flow from metal to the semiconductor these two situations are illustrated in Figure 1.3.
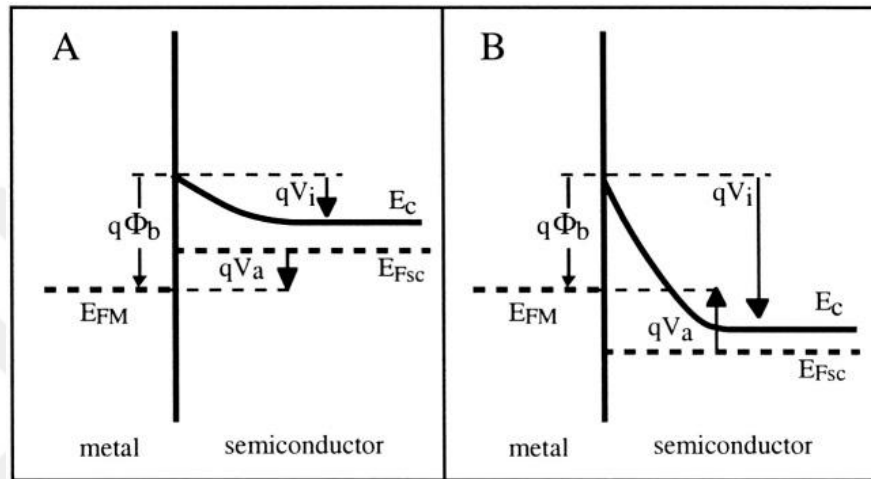
Figure 1.3. Energy band diagram of Schottky diode A) forward biased and, B) reverse biased (Colinge JP and Colinge CA, 2002, p.142).

1.2.3 Extension of the Depletion Region

The width of depletion region of a Schottky contact can be calculate by Poisson equation.

$$\frac{d^2 \emptyset(x)}{dx^2} = -\frac{\rho}{\varepsilon_{sc}} = -\frac{qN_d}{\varepsilon_{sc}} \tag{1.3}$$

$$\frac{d\emptyset(x)}{dx} = \frac{qN_d}{\varepsilon_{sc}} (W - x) \tag{1.4}$$

By integrating the Eq. (1.4) we obtain,

5

$$\emptyset(x) = \frac{-qN_d}{2\varepsilon_{sc}} (W - x)^2 \qquad (1.5)$$

When the potential at x=0 is equal to the potential in the semiconductor side, the width of depletion region becomes,

$$W(V_a) = \sqrt{\frac{2\varepsilon_{sc}}{qN_d} (V_i - V_a)} \qquad (1.6)$$

Where V_a is the applied potential and V_i is the barrier potential. Then using the Eq. (1.4) the electric field at x=0 can be written as,

$$\varepsilon(0) = -\sqrt{\frac{2qN_d}{\varepsilon_{sc}} (V_i - V_a)} \qquad (1.7)$$

1.2.4 Schottky Effect

The Schottky barrier in metal side is not constant by applied potential. Some lowering in ϕ_b is observed. Mirror charges producing in metal by electrons cause this lowering. Thus, the potential barrier is lowered due to the charge which is attracted by metal and semiconductor contact (Coligne JP and Coligne CA, 2002, Chapter 5).

The attraction that exerted by metal on an electron can be calculated and the Coulomb force between these two charges is,

$$F = \frac{-q^2}{16\pi\varepsilon_{sc}x^2} \qquad (1.8)$$

Then the electric field can be represents in the following relation

$$-q\varepsilon_m(x) = \frac{-q^2}{16\pi\varepsilon_{sc}x^2} \qquad (1.9)$$

The potential energy becomes,

6

$$P(x) = -qV(x) = \int_x^\infty \frac{-q^2}{16\pi\varepsilon_{sc}x^2}\,dx = \frac{-q^2}{16\pi\varepsilon_{sc}x^2} \qquad (1.10)$$

The initial potential starts P(x=∞)= 0. Lowering of the barrier potential can be written by the following expression,

$$\Delta\phi_b = \sqrt{\frac{q\varepsilon}{4\pi\varepsilon_{sc}}} \qquad (1.11)$$

By using Eq. (1.6), the Schottky effect becomes,

$$\Delta\phi_b = \sqrt[4]{\frac{q^3 N_d}{8\pi^2\varepsilon_{sc}x^3}}(V_i - V_a) \qquad (1.12)$$

As a result, potential barrier is equal to,

$$\phi_b' = \phi_b - \Delta\phi_b \qquad (1.13)$$

1.2.5 I-V Characteristics of a Schottky Diode

A quantum mechanical process causes the electrons affected the barrier potential between semiconductor and metal. This process called as "thermionic emission". The thermionic emission is triggered by the thermal energy of each electrons. At room temperature non-zero probability to that some electrons bring enough energy to affected on the barrier. When the diode forward biased the thermionic emission becomes,

$$I_{m\to s} = AR^*T^2\exp\left[\frac{-q(\phi_b'-V_a)}{kT}\right] \qquad (1.14)$$

Where R^* is the Richardson constant, A is the area of the diode. By using $I_{m\to s} = -I_{s\to m}$ when applied potential is zero and $I_{s\to m}$ is constant and independent on the applied potential,

$$I_{s\to m} = -AR^*T^2\exp\left[\frac{-q\phi_b'}{kT}\right] \qquad (1.15)$$

7

Then the net current can be written as follows,

$$I = AR^*T^2 \exp\left[\frac{-q\phi_b'}{kT}\right]\left[exp\left(\frac{qV_a}{kT}\right) - 1\right] \tag{1.16}$$

The equation (1.15) represents I-V characteristics of the Schottky diode similar to PN junction. Additionally the current changes with temperature and width of the barrier potential between semiconductor and metal (Coligne JP and Coligne CA, 2002, Chapter 5).

1.3 A Brief Background of Metal-Oxide Gas Sensors

It is known that metal-oxides are sensitive to various gases at high temperatures. This sensing mechanism of the gas sensors are related to the point defects in the bulk structure and the reaction of the oxygen in the gas phase. Changing the atmospheric pressure creates this effect. At low temperature (below $90^{\circ}C$) the variation of the conductivity of SnO_2 and ZnO depends on the adsorption and desorption. In N-type semiconductors, surface reactions depend on the negatively charged O_2 and O_2^-. The relation between the conductivity of metal-oxide structure and partial pressure changing of the oxygen in the atmosphere is shown in the equation below (Çakır, 2014).

$$\sigma = \sigma_0\,exp\left(-\frac{E_a}{kT}\right)P(O_2)^{1/n} \tag{1.17}$$

where T is temperature in Kelvin, k is the Boltzmann constant, E_a is the activation energy of the conductivity of the bulk structure, n is an integer. Under high intensive the oxygen, when it is applied a low density combustive gas inside the media, the resistance of the metal-oxide like SnO_2 is noticeably changed. This formula does not explain this situation because the partial pressure of the oxygen will not be changed. In N-type metal-oxide, adsorbed oxygen formed a depletion region on the metal-

oxide grains. Then a layer that there is no electrons on the surface is occurs (Çakır, 2014).

$$O_2(g) + 2e^- = 2O^- \tag{1.18}$$

The resistance that semiconductor metal-oxide in the atmosphere is high. The length of depletion region can be express by the following equation derived from the Poisson's equation can be written by,

$$L = \frac{q_s}{eN_d}\left[\frac{2K\varepsilon_0\Delta\emptyset_s}{eN_d}\right]^{1/2} \tag{1.19}$$

where $\emptyset_s$ and N_d are the surface change and ionized impurity concentration, K is the static dielectric constant of the oxide, ε_0 is the permittivity of the space, and $\Delta\emptyset_s$ is surface potential barrier length. If $2K\varepsilon_0 = 10^{-12}\,F/cm$, $N_d \cong 10^{19}cm^3$, and $\Delta\emptyset_s = 1V$ the length of depletion region is between 1 nm and 100 nm.

In addition, if the sensor is in under the exposure in the H2 atmosphere, the reaction becomes,

$$O^-(s) + H_2 \rightarrow H_2O + e^- \tag{1.20}$$
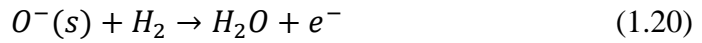
During this process electrons, trapped by the adsorbed oxygen return back into the grains. This causes the resistivity of the oxide decreases and descent in the potential barrier (Çakır, 2014).

The most effected factors to sensing property of the gas sensors are the width of depletion region (L), and size of the grains (D). When D<2L, resistance of the grain dominates the whole resistance of the chain. So, grains control the sensitivity. The sensitivity depends on the size of grains. If that size gets smaller, the sensitivity will be increased. This status is shown in Figure 1.4 (Çakır, 2014).
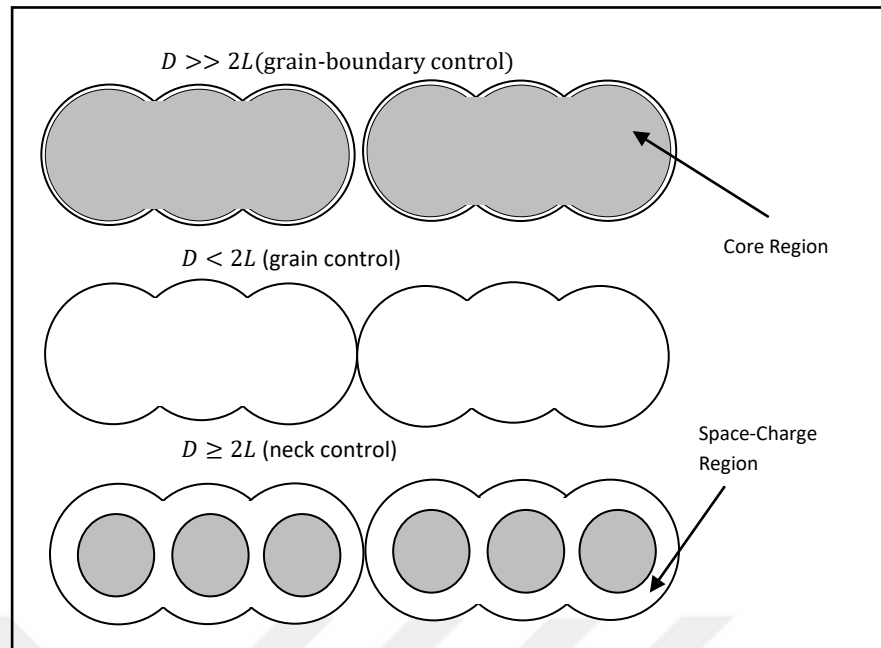
Figure 1.4. Schematic representation of depletion region depending on grain size.

It is possible to form a nano-crystalline material by shrinking the grain size. So, depletion layer and grain size can be same size. Therefore, the oxygen adsorption will be fully depleted. These materials can be use in high sensitive gas sensor production (Çakır, 2014).

1.4 Factors That Affect the Sensitivity of Metal-Oxide Gas Sensors

The ideal sensor must be high sensitive and low sensing limit to work for purpose. In order to increase the sensitivity of metal-oxide materials, there is some important methods, which are growth effect, doping effect, and temperature effect.

1.4.1 Effect of Growth

Due to the forming of depletion region, carrier concentration in width (L) decreases. Three types of conductivity mechanism is obtained, (a) For grown crystalline the grain size is D>>2L and conductivity is forming in grain space-charge region by Schottky barrier, (b) if the grain size (D) is equal to the (2L), each conductivity channel decrease up to effect the total current, (c) if D<<2L, each of

the grain is covered by the depletion region and carrying electron will mostly affected by the charge changing on the surface of the particles (Dey, 2018).
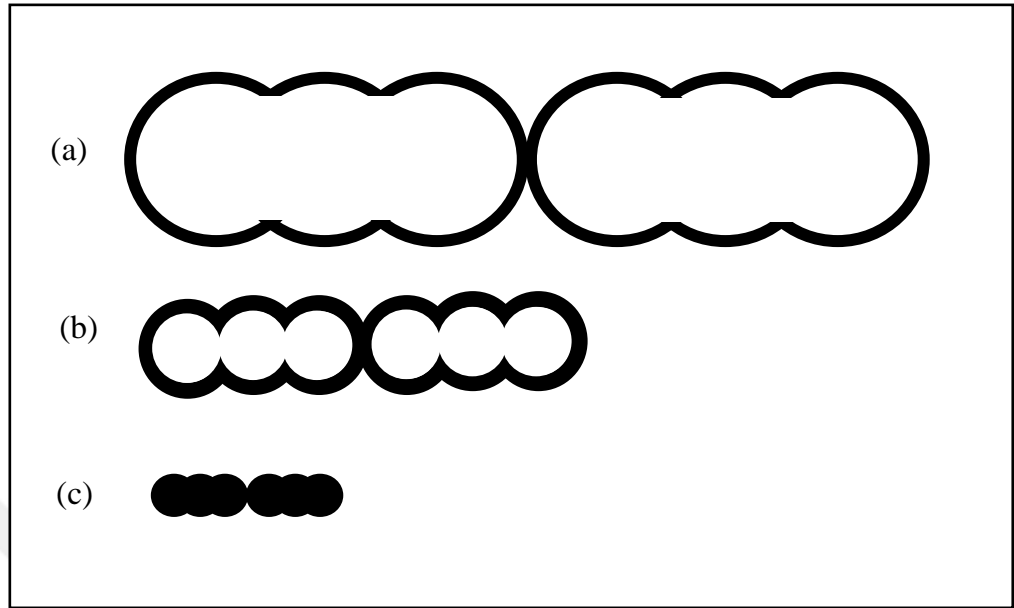
Figure 1.5. The conductivity mechanism in gas sensitive metal-oxide. Black regions represent the high-resistance depletion region (a) $2L \ll D$, (b) $D \geq 2L$, (c) $D \leq 2L$

By decreasing the particle sizes (neck or grain boundaries) that is controlled by the grains and when the conductivity is controlled by the grains the state that the grains are totally covered by the depletion region, is the most ideal situation. Because this situation provides high resistance range.

For a different metal-oxide, the depletion region can be change about 1nm to 100nm. In a granular structured metal-oxides, the depletion region which is formed on grains, causes the creation of Schottky barriers between oxide crystalline. Conductivity can be changed by the concentration of the oxygen in the surface (Bochenkov and Sergeev, 2010).

1.4.2 Effect of Doping

The sensitivity of metal-oxide gas sensors can be increased by doping of metals i.e. Palladium (Pd), Gold (Au), Platinum (Pt), Copper (Cu), Cobalt (Co). The

doping can be applied on the surface or whole the volume. Although the doping used in commercial products and it is a traditional method, it is not understood that how to doping works (Bochenkov and Sergeev, 2010).

SnO_2 is commonly used in this field. Interaction between gas and metal-oxide is fast enough when the temperature 100^oC. Electron interaction between the conduction band of the metal-oxide and adsorbed gas molecules is too fast to not affect to the kinetic interaction (Korotcenkov, 2007).

Noble metals have high catalytic activity and this property of noble metals can be used for increase the reaction in the surface of the sensor. In order to doping these noble metals onto the material some techniques can be use such as, sol-gel, sputtering, and vapor deposition (Çakır, 2014).

1.4.3   Effect of Temperature

The temperature is another important parameter for metal-oxide gas sensors. Gas sensing property is typical for most of the gas sensor.

Table 1.1. Some example for tin-oxide based sensors (Eranna et al, 2004).

Tin-Oxides with additives & dopants	Sensing gas	Operating Temperature Range (^oC)	Range detection limits	Sensing element form
SnO_2-Pt	CO	150 - 300	400 - 1000 (ppm)	Thin films on oxidized silicon substrates
SnO_2-Pd/Pt	CO	Room temperature to 500	250 - 1000 (ppm)	Thick films onto alumina substrates
SnO_2	CO NH$_3$	450 - 500	100 - 1000 (ppm)	Microelectronic sensor structures
SnO_2	NO$_2$	150 - 200	0 - 800 (ppb)	Thin films on alumina substrates

Sensitivity increases directly proportional to the temperature. Then at a certain temperature sensitivity is maximum value. We can say that a gas sensor has the maximum sensitivity at this maximum value. Thus each of the metal-oxide gas sensors have their own operating temperature (Çakır, 2014).

When the activation energy of the chemical reactions high, the sensor response is limited by the rate of the chemical reaction. At a certain temperature range, reaction rate and diffusion rate get equal and at this temperature range the sensor response get its maximum value. As we see in Table 1.1 each material have their own operating temperature. The material cannot sense the gas except its operating temperature effectively (Eranna et al, 2004).

1.5   Characterization of MOS Structures

In order to characterize MOS structure some techniques such as Scanning Electron Microscopy (SEM), X-Ray Diffraction (XRD), Energy Dispersive Spectroscopy (EDS), Fourier Transform Infrared Spectroscopy (FTIR), are use. This section consists of the steps of fabrication process and technical information about the methods to characterize our metal-oxide gas sensor and electrical measurements that examine the sensitivity of the sensor.

1.5.1   Scanning Electron Microscopy (SEM)

Scanning Electron Microscopy (SEM) is a kind of microscope which scans the surface of the sample and takes the image of the surface by focused electron beam. Electrons interact with the atoms in the sample and produces different topographical information from the surface of the sample.

In a scanning electron microscope, an electron gun is used for create an electron beam and in order to focus the beam, magnetic coils are used. In addition, to scan the electrons that scattered from the surface of the sample, there is scanning coils, and in order to scan these scattered electrons vertical and horizontal, there is also electron detectors for this (Poole and Owens, 2003, Chapter 3).

The resolution can be reach higher than 1 nm with SEM. Standard SEM devices are proper to examine dry and conductive surfaces in vacuum. To accelerate the electrons, electron gun, anode plate, and scopes which are used for focus the beam, must be in a high vacuum around 10^{-4} Pa. However there is also SEM devices that can take the image of the liquid samples at low vacuum (Poole and Owens, 2003, Chapter 3).

The quality of the lenses is not only the factor which limited the maximum resolution. The real factor is the wavelength of the light. The visible wavelength of the light is between 400nm and 700 nm. The wavelength of the UV light is between 200 nm and 350 nm. Thus, in theoretical, the resolution of light microscopes are limited by the wavelength at these intervals. SEM uses electron instead of the light. Because of this SEM is more advantageous. Because the wavelength of the electron is smaller than the wavelength of the light (Öztel, 2018).

1.5.2   Energy Dispersive Spectroscopy (EDS)

In a SEM device, when the electron beam that is formed by the electron gun, attracts with the sample, there will be characterized X-Rays will appear from the sample. It is possible to analyze the chemical properties with EDS (Öztel, 2018).

There is also detector which collects X-Ray from the samples. EDS measurements can be taken in a short time interval. In a small area about 1 μm, the SEM device detects what kind of elements are there and how they change in different region (Öztel, 2018).

1.5.3   X-Ray Diffraction (XRD)

In 1895 Wilhelm Roentgen was obtained light beam by scattering high-energy electrons into a metal target. He could not understand the nature of these rays and he called them as "X-Ray".

The wavelength of X-Ray is between in the range 0.1 nm - 0.001 nm. The wavelength of X-Ray is 1000 times shorter than the wavelength of the visible light. That is why their energies are 1000 times larger than the visible light.
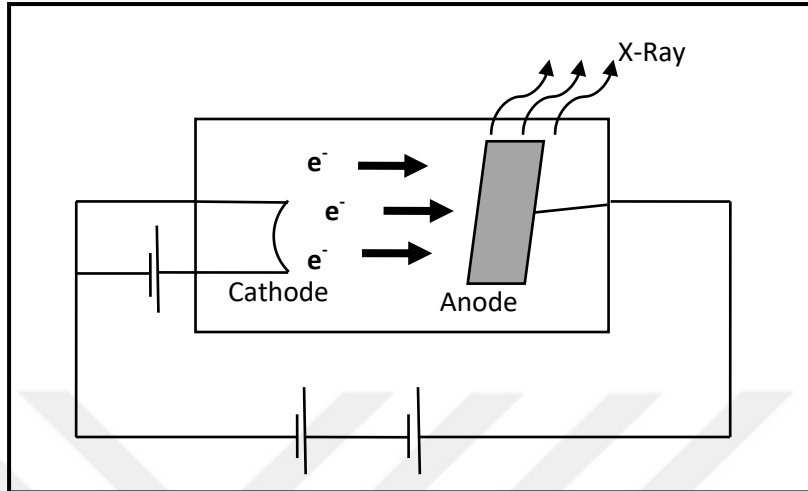
Figure 1.6. Illustration of an X-Ray tube

The Figure 1.6 shows the schematic of an X-Ray source. When cathode is heated, there is going to be free accelerated electrons from cathode to anode tungsten target. The applied potential difference between cathode to anode causes this movement. With this energy, electrons reach at the speed 0.1c.

When the electrons hit the target X-Ray which is perpendicular to the moving electrons is created (Öztel, 2018).
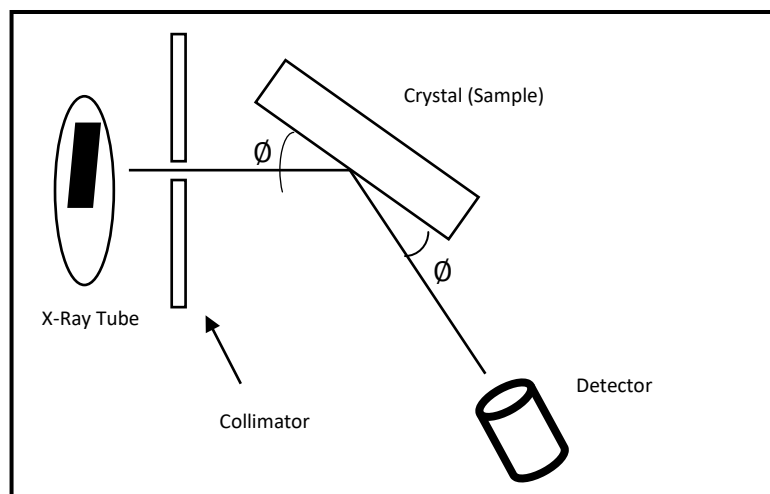
Figure 1.7. Schematic of X-Ray spectrometer.

As we see in Figure1.7 in X-Ray spectroscopy incident beam is rectified by collimator then it is provided that the beam routed into the crystal sample. Then the intensity of the reflected beam is measured by a detector. By changing the angle of the detector or rotating the sample a spectrum will be obtained. With this spectrum the crystal structure is determined (Öztel, 2018).

1.5.4 Fourier Transform Infrared Spectrometry (FTIR)

The spectrometers based on monochromator and slit systems are very useful instruments for measurements of permeability and absorption spectrum in the range from UV to near infrared spectrum. In the contrary, they are not useful in middle and far infrared regions. The use of Fourier-transform infrared spectrometry in these regions is more convenient and efficient. In addition, Fourier-transform spectrometry has a high output rate which means it gives sharp and clear results (Sardela, 2014, Chapter 2).
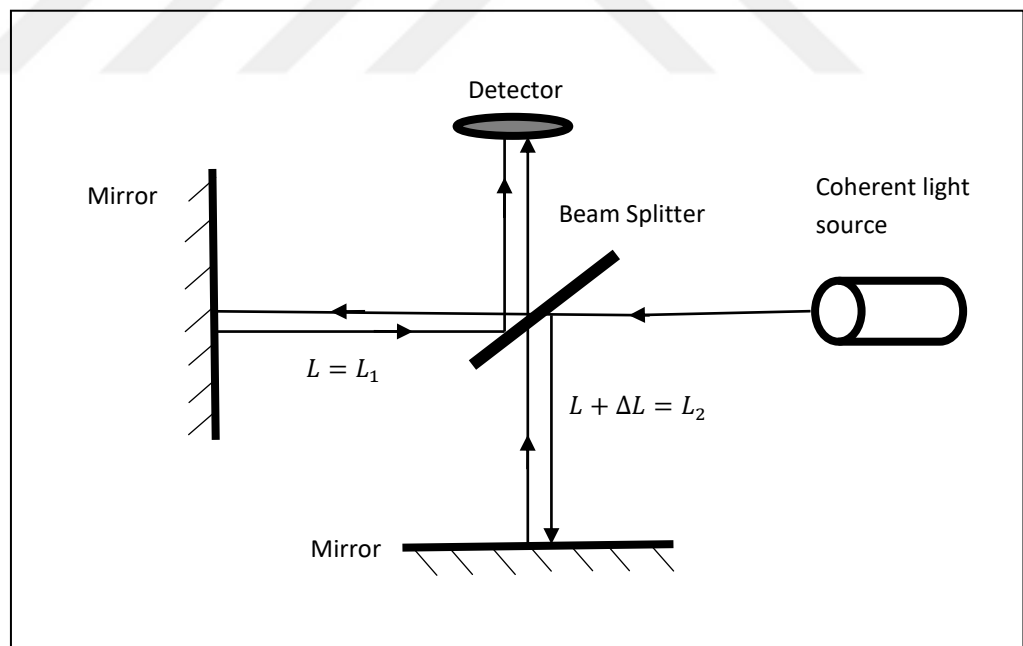
Figure 1.8. A Michelson-Morley Interferometer.

Photon energy in the infrared region usually interacts with phonon as well as molecular vibrations and rotations. This situation depends on the atomic structure of

the material and hence Fourier-transform infrared spectroscopy (FTIR) is a very useful instrument for understanding the structural properties of the material.

2. AIM AND SCOPE OF THE STUDY

Tin-oxide based gas sensors were produced and annealed at $600^{o}C$. Then, the thin films were characterized by X-Ray Diffraction (XRD), Scanning Electron Microscopy (SEM), I-V characterization, and Fourier Transform Infrared Spectroscopy (FTIR).

In the second step of the fabrication process, Platinum was doped on the surface of SnO_2 for certain times and annealed. The effect of the Pt doping on the surface were examined by same techniques; SEM, XRD, I-V, and FTIR. Then produced doped and undoped SnO_2/SiO_2 thin film structures were investigated for gas sensor applications by electrical measurements in under the different gas concentration of O_2.

3. MATERIALS AND METHODS

Before sensitivity measurements had been taken completely, in order to decide which material need to use in this study was determined. TiO_2 and SnO_2 based gas sensors were produced and annealed at $400^{o}C$, $600^{o}C$ and $800^{o}C$, respectively. Best result was observed in tin-oxide based sensor which annealed at $600^{o}C$ and that is why the best sensitive sensor has been chosen. The TiO_2 based films were high resistive at room temperature. However, SnO_2 based films were much more sensitive to low concentration of O_2 gas. And It is known that SnO_2 is one of the best sensitive material in low concentration of gases, thet is why SnO_2 based sensors are commonly used in gas sensors applications (Tangriela et al, 2017). In addition SnO_2 is an N-Type semiconductor (Oyabu, 1982). And SnO_2 has wide bandgap (3.6eV) semiconductor (Ling et al, 2017).

3.1   Fabrication of the Device

The tin-oxide based metal-oxide Semiconductor gas sensors were fabricated in Nuclear Radiation Detector Research and Application Center (NRDC), Bolu Abant İzzet Baysal University Bolu, Turkey. 6 inches N-type Silicon wafers with resistivity 1-4 ohm-cm were used at start. The shadow-mask was designed by me. The process details will be given in next sections

3.1.1   Wafer Cleaning

Presence of any contamination on wafers causes significant leakage current for the fabricated devices; therefore standard Radio Corporation America (RCA) was used as cleaning procedure. RCA procedure has three chemical steps which are;

a) Organic Cleaning: In order to clean organic contamination by using 5:1:1 DI - H_2O: H_2O_2: NH_4OH

19

b) Ionic Cleaning: To clean ionic contamination by using 6:1:1 DI-H_2O: H_2O_2: HCl

c) Oxide Cleaning: In order to indigenous SiO_2 layer can grow in the surface of the wafer. This contamination was removed from the surface with 100:1 DI-H_2O: HF solutions.

Afterwards the RCA cleaning process by using pure nitrogen wafers were dried.

3.1.2   Field Oxide Growth

In diffusion furnace, the field oxide layer was grown on the cleaned Si wafer. In order to deposit SiO_2 layer into the Si wafer the wet oxidation technique was followed.

The Figure 3.1 represents the schematic diagram of the sample after SiO_2 is grown on the Si substrate. Then the thickness of the layer was measured and found to be $1 \mu m$.
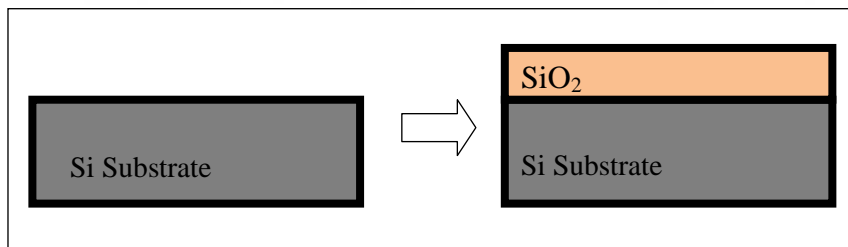

Figure 3.1. Field Oxide Growth.

SiO_2 layer was grown on the silicon wafer at $1000^{o}C$ in (Qingdao Sun Red Electronic Equipment Co.) diffusion furnace in 20 min. By using hydrogen and oxygen gas the wet oxidation were completed. The oxide growth explained by the following equation.

$$Si + 2H_2O \rightarrow SiO_2 + 2H_{2(g)} \tag{3.1}$$

3.1.3 SnO$_2$ Deposition

One of the most preferred physical vapor deposition method is evaporation by electron beam (e-beam). The e-beam evaporation makes fast and high purity coating possible. In this method the electron beam is routed on the target material. The kinetic energy which is formed from electron beam is converted on a thermal energy and provides the source material to be evaporated. The atoms or molecules were deposited on the target with gained kinetic energy in vacuum.

The coating of the pure elements, compounds, and alloys is possible by this method. Since the material to be coated is heated directly, It is not possible to evaporate the crucible material. To maintain purity in coatings, the melting temperature of the selected crucible material must be high and the vapor pressure is low. Since the coating material follows a straight path, the side walls on the substrate do not coated by the material in this method. That is why the photolithography obeys the lift-off technique.

After the field oxide grown in Si layer, SnO$_2$ was deposited on the material by e-beam evaporation (electron beam evaporation). In under pressure 7×10^{-4} Pa to 1.1×10^{-4} Pa SnO$_2$ was deposited in the surface. Until the thickness reached at 120 nm. Then the thickness was measured again then 130 nm observed.
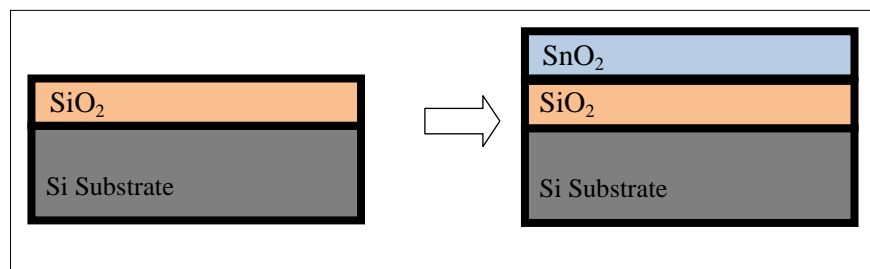
Figure 3.2. Schematic representation of deposition of SnO$_2$.

After that, obtained material annealed at 300°C, 450°C, and 600°C. The annealing process had taken 30 minutes. The Figure 3.2 shows the schematic representation of deposited SnO$_2$ upon the SiO$_2$ substrate the tin-oxide sensing layer was deposited on SiO$_2$ in (Dong Guan Plasma Electronic Equipment Co).electron beam evaporation system. During the process the following parameters were set;

Filament current was 120mA, substrate temperature was 250°C and, deposition rate approximately 1.0 nm s^{-1}.

3.1.4 Pt Deposition and Annealing Process

After SnO$_2$ was deposited, the samples were characterized. By using sputtering technique the material that we had before was doped with Pt in the order; 1 second, 3 seconds, and 5 seconds. Sputtering technique is one of the best technique used for thin film deposition and etching. The radiofrequency (RF) power was at 300 W for the deposition procedure.
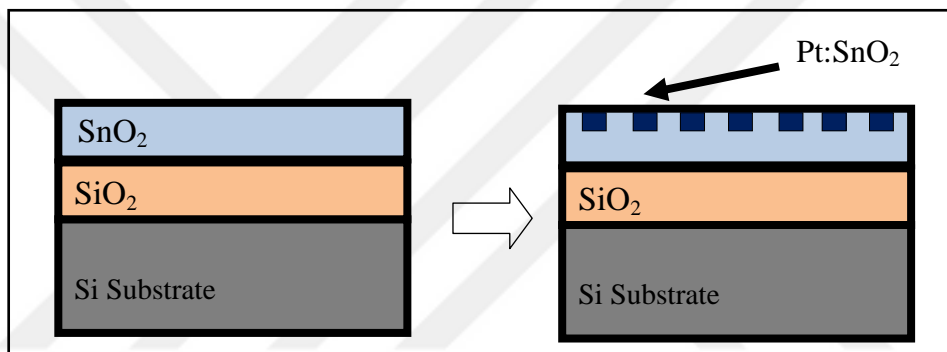
Figure 3.3. Pt deposition on SiO$_2$ surface

The initial pressure of the sputtering chamber was $1,5 \times 10^{-6}$ torr and held at 5×10^{-3} torr during the doping Pt on the target under Argon gas.

3.1.5 Inter-digitized Contact Formation

The shadow mask was used to deposit the Pt contact on the metal-oxide based sensor. The shadow mask is a metal sheet behaves like a barrier in front of the target in sputter during the sputtering process to thin film deposition. The mask allows the electrons can pass through the holes on the metal sheet. Figure 3.4 shows the schematic representation of the mask after the process is finished.

According to Lee (2017)," The interdigitated geometry is the most widely accepted geometry for the electrodes of a gas sensor since it enables a wide contact area between the electrodes within the limited area. In addition, it forms the electrodes first and then deposits the sensing materials on them, thereby causing no damage to the sensing materials" (p. 2). Therefore, the interdigitated geometry was chosen for this study.
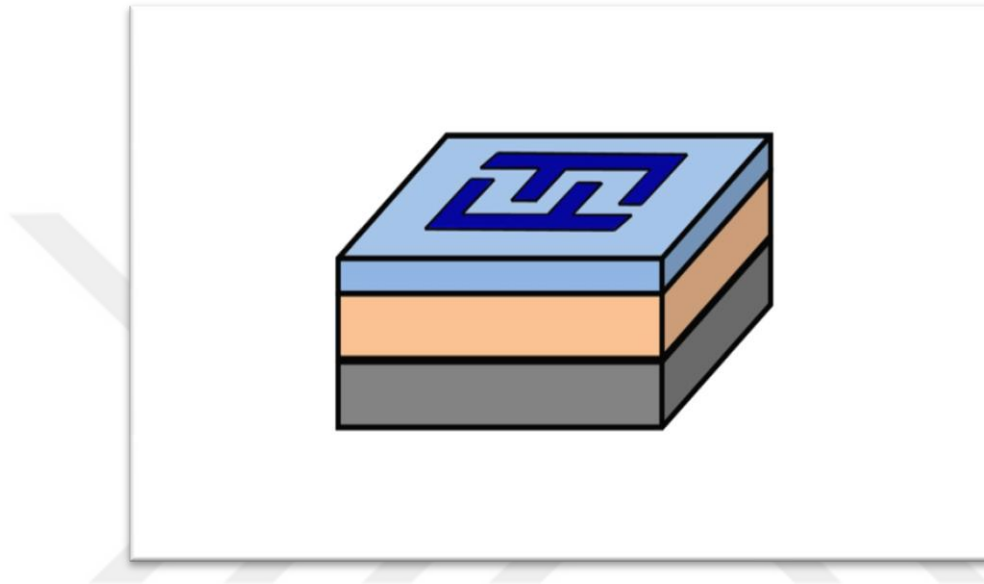
Figure 3.4. Schematic illustration of the produced tin-oxide based gas sensor

The size of the sensor is given in the Figure 3.5. The mask designed by myself and the 2mm length was determined. After 1 sec, 3 secs, and 5 secs Pt doping the designed shadow mask was put on the material as a barrier then sputtered again, but this time Pt deposition applied by the shadow mask. The Pt deposition our designed mask appeared on the thin film just illustrated in Figure 3.4. Another technique in order to apply mask on the thin film target is the photolithography.
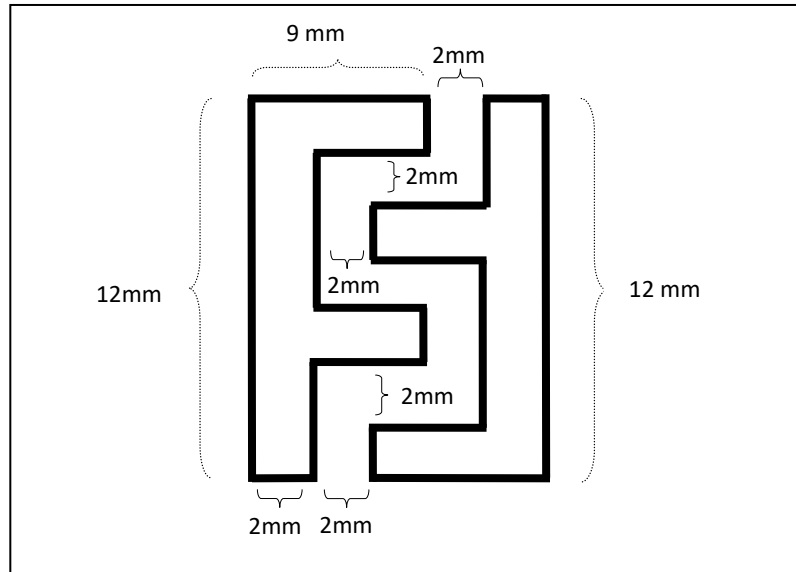
Figure 3.5. Sizes of the designed shadow mask.

3.1.6   Device Characterization

After the fabrication of Metal-oxide Semiconductor gas sensor device, to characterize the material XRD, SEM, EDS, FTIR, and I-V characteristics were observed.

Figure 3.6. Rigaku Multiflex X-Ray Diffractometer in BAIBU, Bolu-Turkey.

The structural properties of SnO_2 thin films were measured by Rigaku Multiflex X-Ray Diffractometer in Bolu Abant İzzet Baysal University (BAİBU), Bolu, Turkey. XRD patterns were obtained between 20° and 60° with a speed 3°/min for all the deposited thin films which were fabricated.

In this study EDS measurements and SEM images were taken by Zeiss EVO HD15 device in Middle East Technical University, Center for Solar Energy Research and Applications (GUNAM), Ankara, Turkey.

In addition, FTIR spectrum anaylsis of the films were recorded with Perkin Elmer Spectrum Two IR-ATR Spectrometer in the range between wavelengths of 400-4000 cm^{-1}, in Bolu Abant Izzet Baysal University, Chemistry Department, Bolu/Turkey.

3.1.7   Experimental Setup

In order to test the gas sensing property of the produced SnO_2 thin film the experimental setup was prepared in NRDC in BAIBU, Bolu, Turkey. Figure 3.7 shows the experimental setup for testing the device in under different gas concentrations.

First, by using the vacuum system the test chamber was taken in under vacuum until the oxygen was decontaminated from the chamber. Then, the test chamber filled with N_2 gas and the hot plate set at certain temperature value and waited till the system get in thermal equilibrium
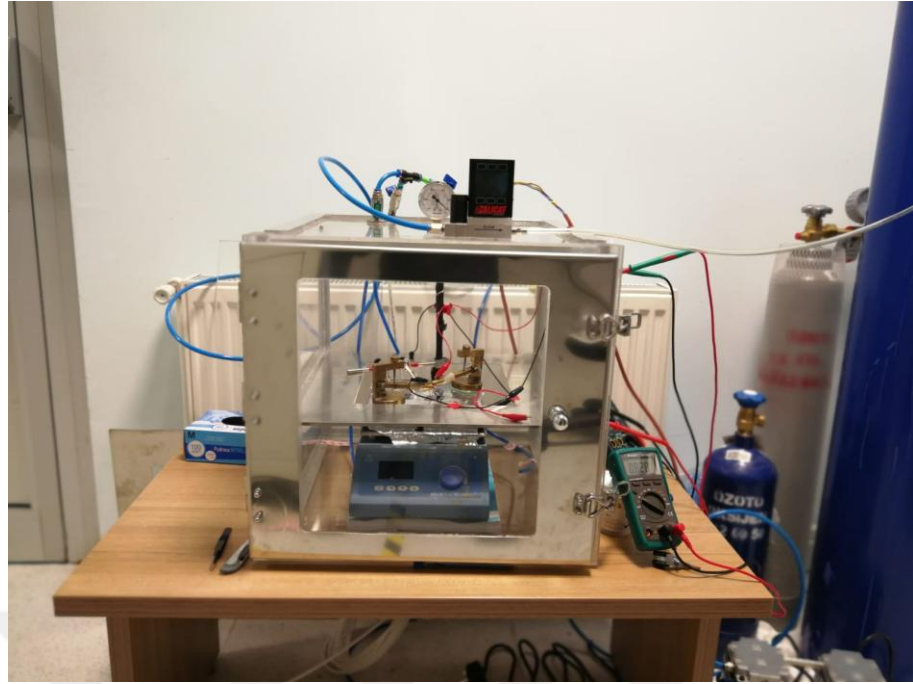
Figure 3.7. The experimental setup to test the device.

In this study N_2 gas used as reference gas. At this time the resistance under the N_2 gas recorded as reference. After that the oxygen gas was started to flow in the test chamber in different concentrations (500, 1000, 2000, 3000, 4000) ppm, and resistance values were recorded several time intervals for each concentrations. Figure 3.8 shows the schematic diagram of the experimental setup.

Figure 3. 8. The schematic diagram of the experimental setup.

The SnO$_2$ thin film which annealed at 600°C and Pt doped thin films were tested at different temperatures; 100°C, 150°C, and, 225°C. The sensor was heated by a hot plate to reach these temperatures. The sensitivity was measured for all the samples that were used in this study.

4. RESULTS AND DISCUSSIONS

4.1.1   XRD Results of Tin-Oxide Based Gas Sensor

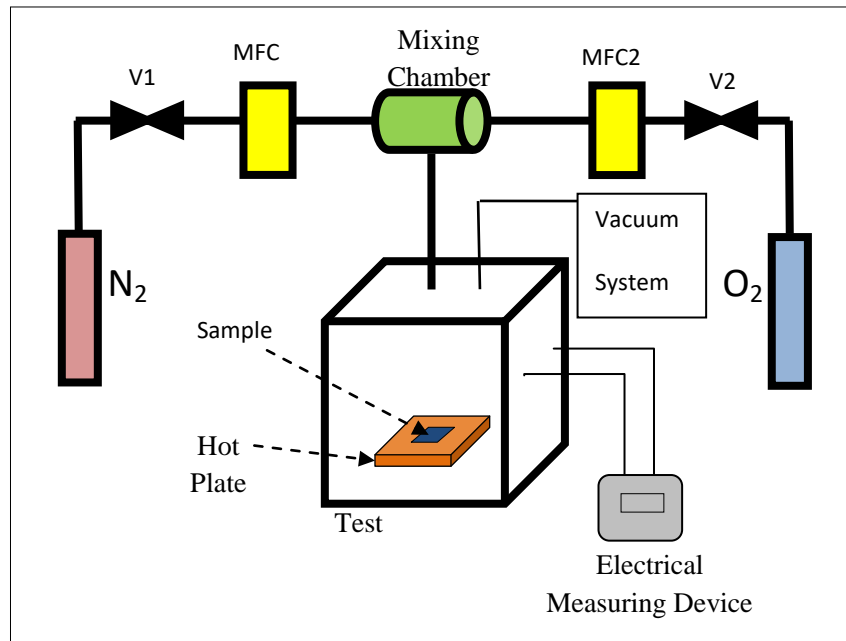The XRD patterns of Virgin (SnO_2/SiO_2 annealed at $600^{o}C$) and 1 second, 3 seconds, and 5 seconds respectively Pt doped thin films in same material was examined. Observed XRD patterns and peaks were compared with International Center for Diffraction Data software.

The observed XRD patterns are shown in the Figure 4.1 states that the XRD patterns of the SnO_2/SiO_2 thin film annealed at $600^{o}C$
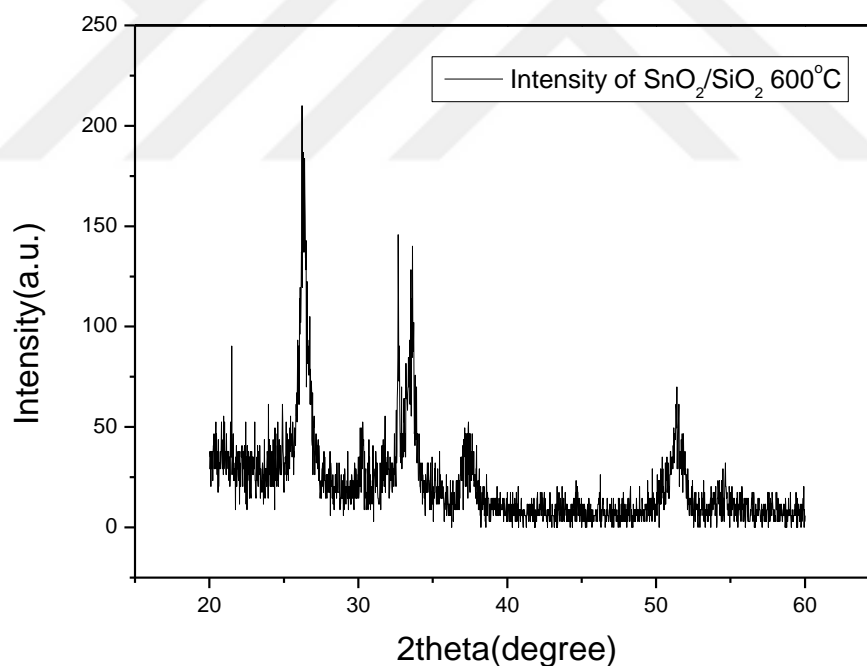
Figure 4.1. XRD Patterns of SnO_2/SiO_2 thin film annealed at $600^{o}C$.

In fabrication process after SnO_2/SiO_2 thin film annealed at $600^{o}C$ Pt was deposited on the thin film in the order of 1 sec, 3 secs, and 5 secs Figure 4.2 shows theXRD patterns of the 1 second Pt doped on the thin film.

28
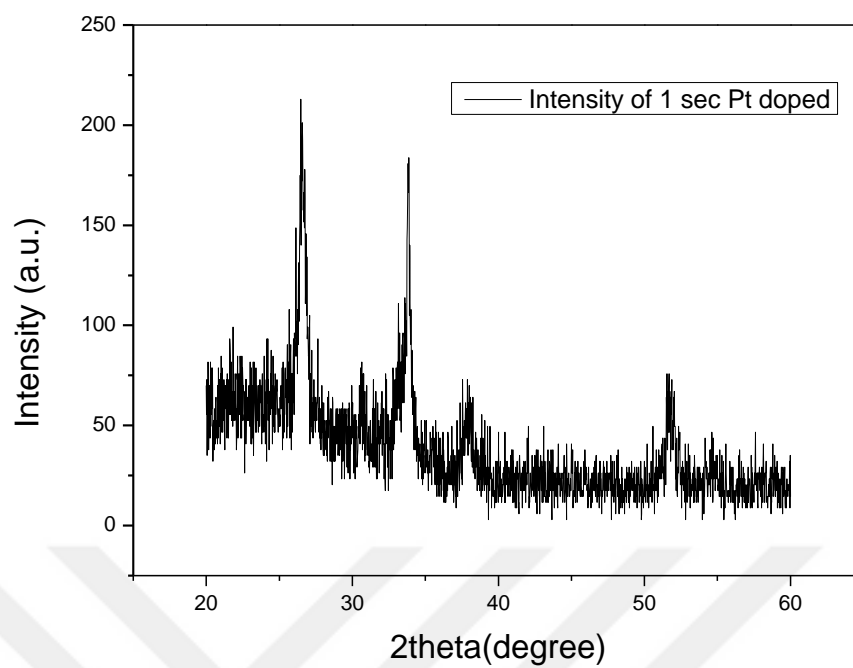
Figure 4.2. XRD Patterns of 1 second Pt doped SnO_2/SiO_2 thin film.
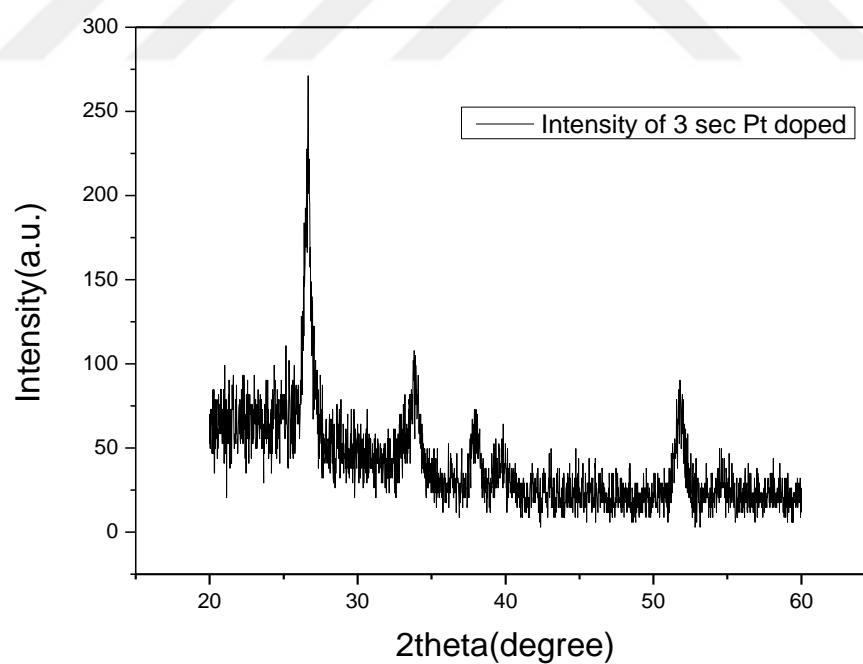
Figure 4.3. XRD Patterns of 3 seconds Pt doped SnO_2/SiO_2 thin film
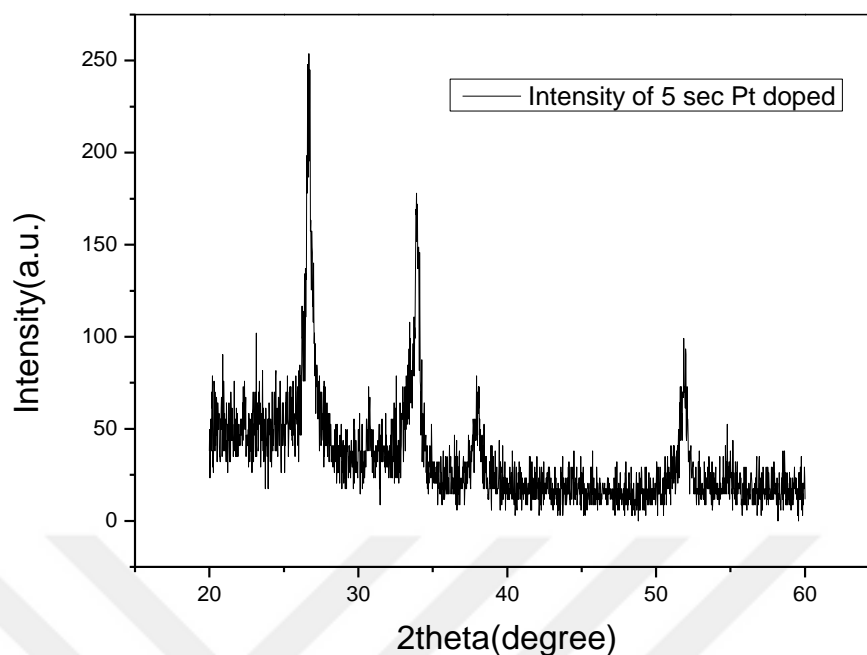
Figure 4.4. XRD Patterns of 5 seconds Pt doped SnO_2/SiO_2 thin film.

Then the XRD patterns of the SnO_2 thin films in order of 3 seconds and 5 seconds Pt doped shown in Figure 4.3 and Figure 4.4.

Sensor efficiencies were closely attached to the microstructure of the layer (Wang et al, 2010). Consequently, the crystal structure of the SnO_2 thin film was analyzed before Pt was doped on the thin film and after the Pt was doped on the thin film by an order. The Figure 4.5 represents the XRD patterns of thin films in each situation. As mentioned before XRD patterns were investigated and marked by International Center for Diffraction Data (ICDD) software.

Superiority of the obtained XRD peaks are similar to the tetragonal phase of - the tin-oxide (ICDD card no: 77-0452). The vestigial two peaks at 30.43^{o} and 32.77^{o} with low intensity are matched with the tin-oxide in triclinic phase. The XRD results shows the two phase structure of tin-oxide are together.

Existence of the reflected peaks of the tetragonal form indicates that the tetragonal phase leads the crystallographic structure of the tin-oxide based virgin thin film.
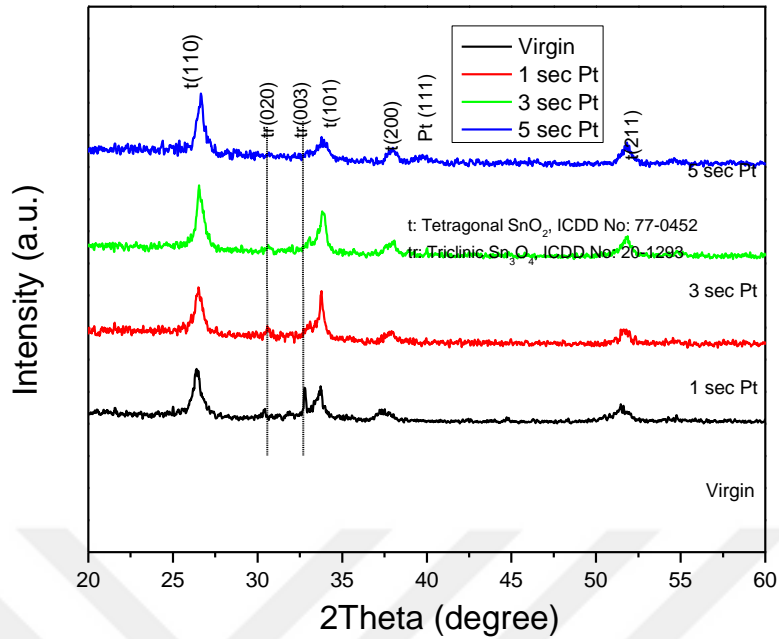
Figure 4.5. XRD patterns of SiO_2 each of the produced thin films

In the angle 26.39^0, the peak angle of the (110) is obtainable, In literally, the standard tetragonal phase of the tin-oxide should be 26.48^0 (checked from ICDD card no: 77-0452) (He et al, 2019; Matylitskaya et al, 2007).

The second phase can be generate an additional stress and strain over the thin film. Another words, the Pt doping on the surface of the thin film has an important effect on the crystalline structure of the tin-oxide layer. By increasing the concentration of the Pt doping the second phase could not be detected. Table 4.1 represents the peak angles of the (110) plane.

Table 4.1. Some characteristics of SnO_2 thin film annealed at 600^oC and Pt doped films in time ordered

Sample	Peak Angle (Degree)	Grain Size (nm)	Lattice Strain	Atomic Concentration of Pt (%)	Resistance (ohm)
Virgin	26.40	27.1	0.0056	0.0	606
1 sec Pt	26.50	20.4	0.0074	0.42	990
3 sec Pt	26.54	20.1	0.0075	0.45	1156
5 secs Pt	26.63	19.2	0.0078	0.58	1939

31

This variety may be related with the variety o the mean surface free energy in the existence of the Pt. The crystal structure changes by the amount of the surface free energy that is obtained with high-temperature annealing in this study (Ohring, 1992, Chapter 1).

When Pt atoms were sputtered onto the tin-oxide surface these atoms diffused on the SnO_2 layer after the thin film is annealed at 600^oC, Pt atoms spreads into the lattice points of the tin-oxide structure and surface free energy is shared between Pt, Sn, and O atoms (Degler et al, 2016).

The ionic radius of Sn is 0.690Å and Pt is 0.625Å (Ahrens, 1952). The crystallite size (P) and lattice strain can be found to be Scherer's formula Equation 4.1 (Scherer, 1918).

$$P = \frac{0.9\lambda}{\beta Cos(\theta)} \quad \text{Scherer's Formula} \tag{4.1}$$

The lattice strain (ε) was calculated with the tangent formula Equation 4.2 (Mishra and Sahay, 2012).

$$\varepsilon = \frac{\beta}{\beta Cos(\theta)} \quad \text{Tangent Formula} \tag{4.2}$$

where β is the FWHM of the XRD peaks respect to (hkl) plane, and the wavelength of the incident beam that used in this study is $\lambda = 1.54$ Å. Calculated values are listed in the Table 4.1. Then calculations shows that by increasing the Pt doping concentration on the surface lattice strain is also increase. By the way, the grain size decreases while the Pt concentration is increased.

4.1.2 Scanning Electron Microscopy (SEM) Analysis

Scanning electron Microscopy (SEM) was utilized to investigate the morphology of SnO_2 layer before Pt was doped on the surface and shortly after the Pt concentration was changed. The effect of the Pt concentration was also examined with the Energy Dispersive Spectroscopy (EDS).

Each of the tin-oxide thin films have various micro-structured polycrystalline phases. The phase difference of the various oxidized Sn variety could be formed. The tin-oxide which annealed at 600^oC has unreliable shapes and non-uniform size. In Figure 4.6, some regions are more luminous than the others. Sn_3O_4 is another phase of Sn and O. Thus, tin-oxide may cause forming these bright sides in Figure 4.6. The doped Pt changed the formation of the surface of the thin film. The grain size may increase until 200 nm according as the doping concentration of the Pt. These increasing can be featured to the collection of grain boundaries of the doped thin films in the existence of the high-interfacial tension (Fliegel et al, 1994).
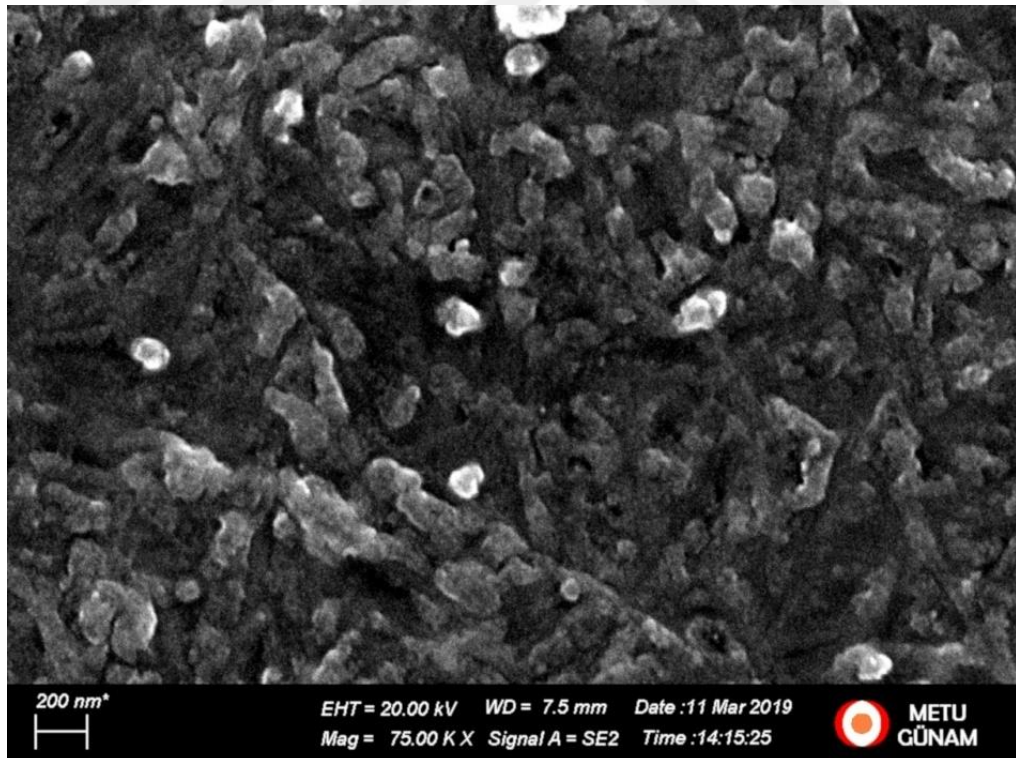
Figure 4.6. SEM image of SiO_2 thin film annealed at 600^oC

33
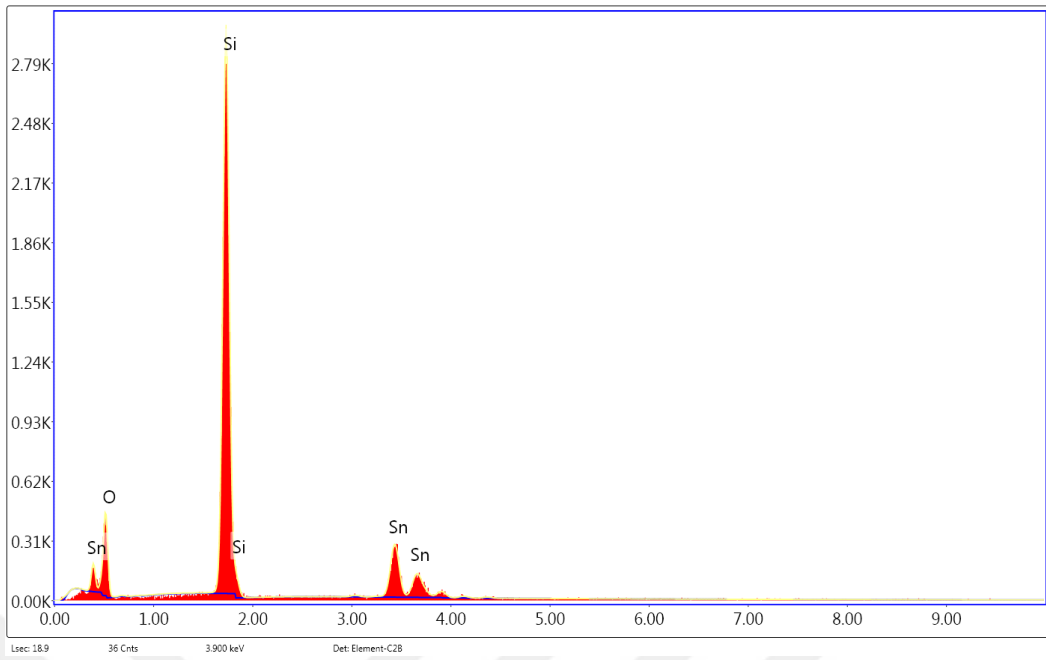
Figure 4.7. EDS results of SiO_2 thin film annealed at 600^oC
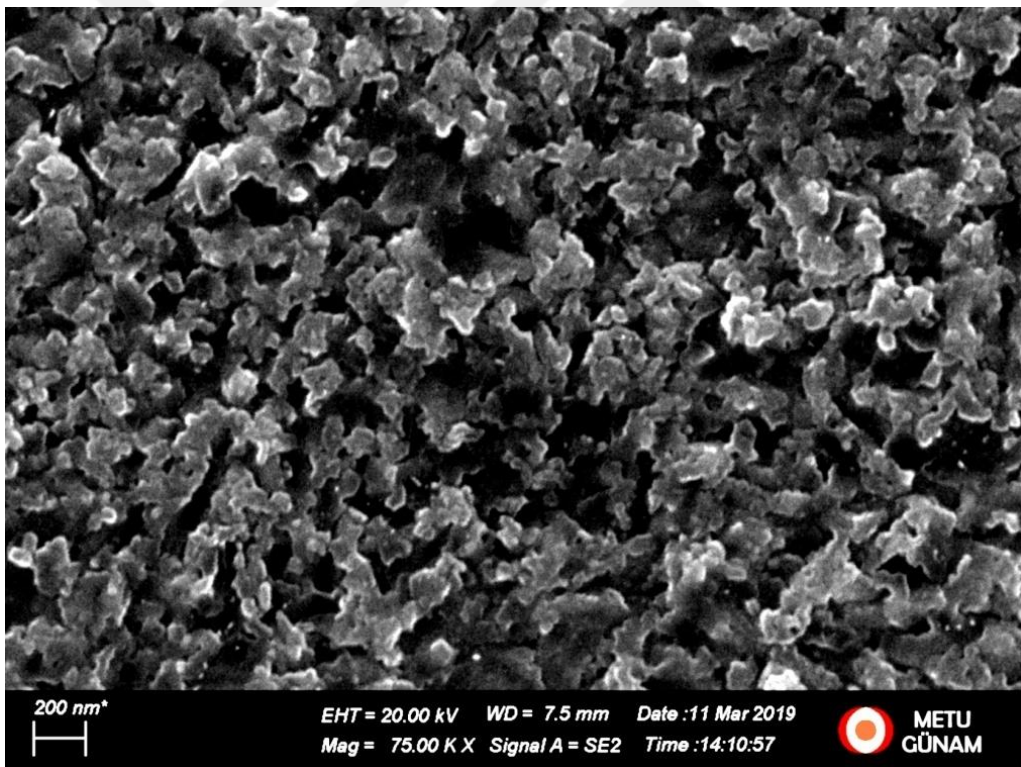
Figure 4.8. SEM image of 1 second Pt doped SnO_2 thin film.
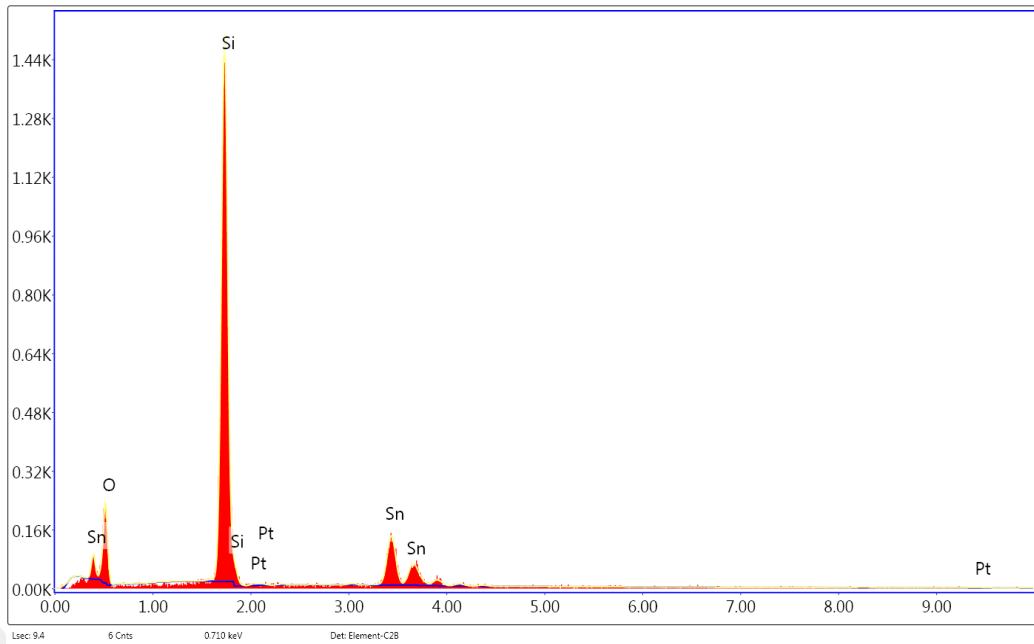
Figure 4.9. EDS results of 1 second Pt doped SiO_2 thin film.
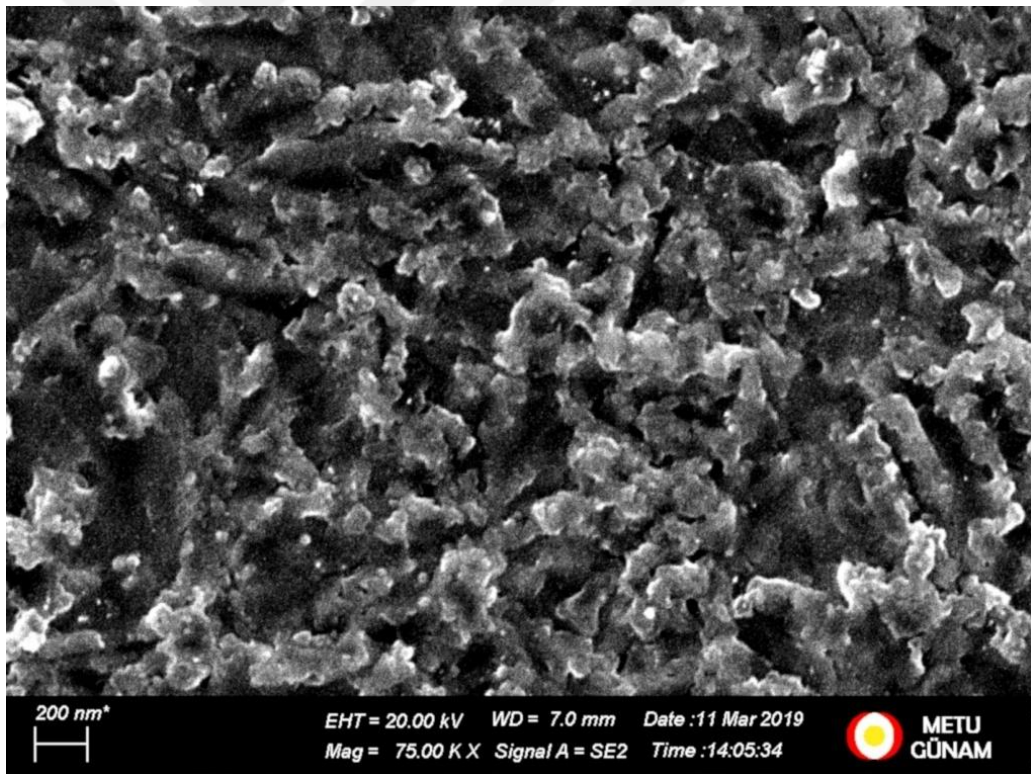
Figure 4.10. SEM image of 3 seconds Pt doped SnO_2 thin film
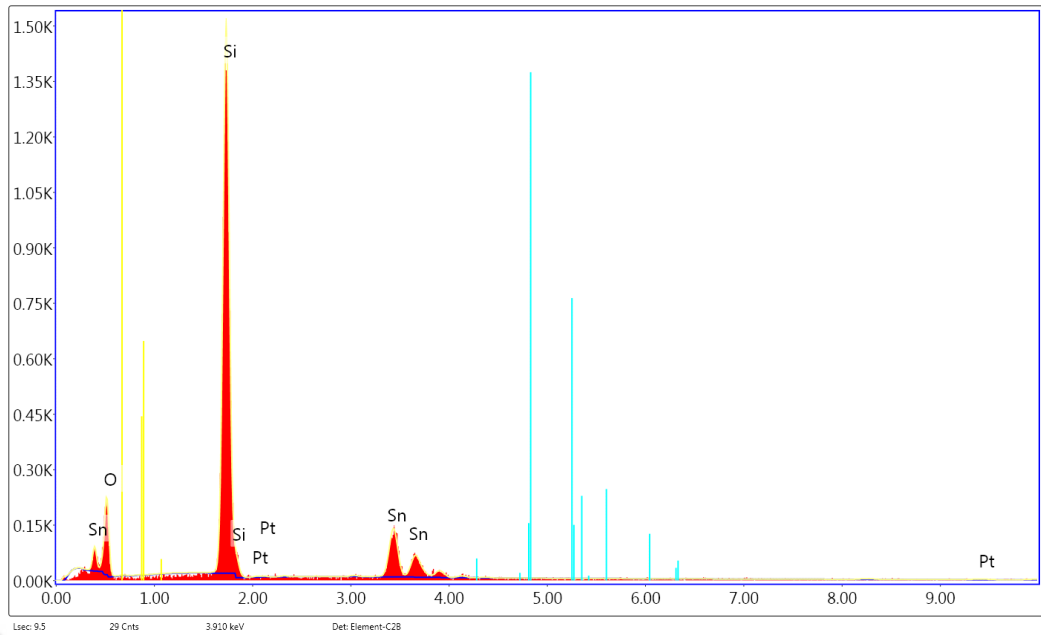
Figure 4.11. EDS results of 1 second Pt doped SiO_2 thin film.
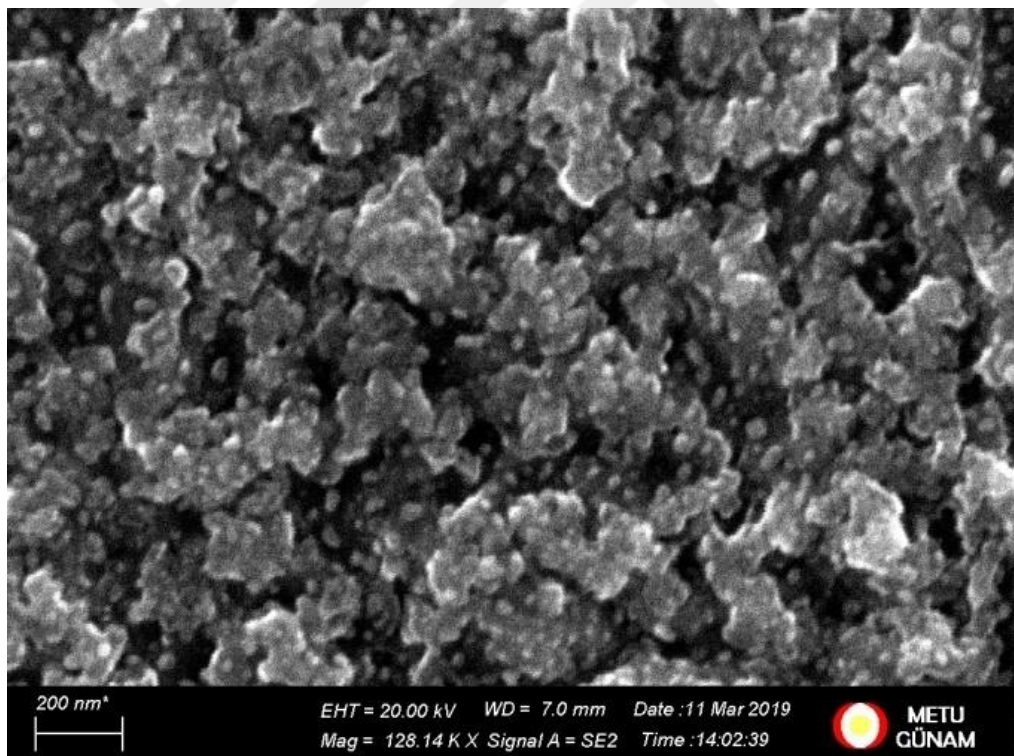
Figure 4.12. SEM image of 5 seconds Pt doped SnO_2 thin film.
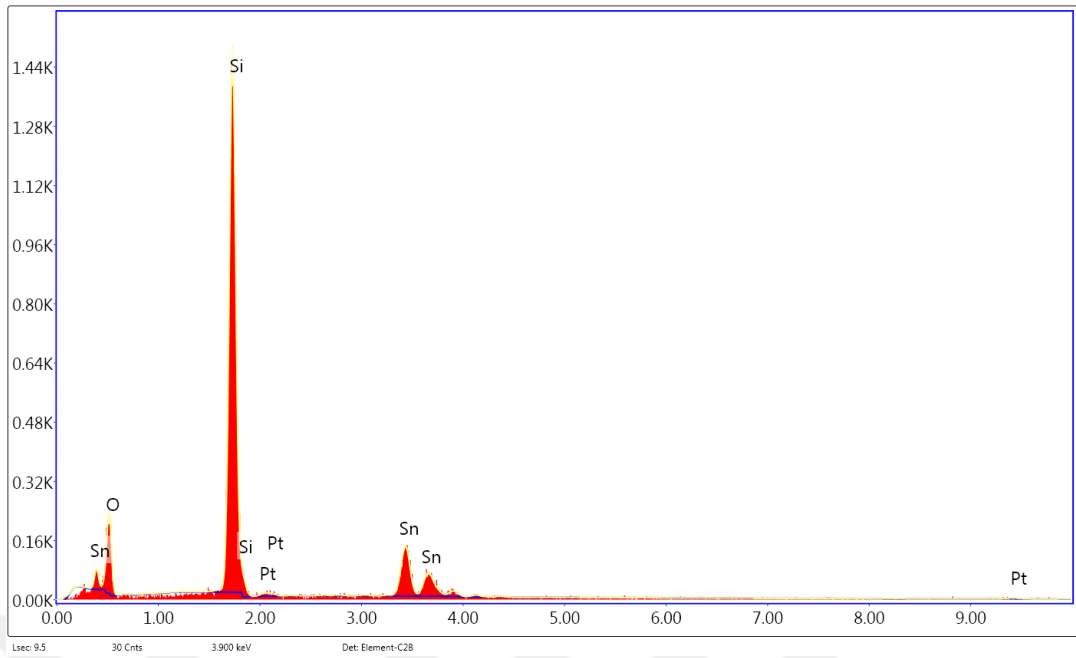
Figure 4.13. EDS results of 5 seconds Pt doped SiO_2 thin film.

Table 4.2. The data table for EDS result of SiO_2 thin film annealed at 600^oC.

Element	Weight (%)	Atomic (%)
O	17.94	11.40
Si	56.71	4.25
Sn	23.35	6.29
Pt	0	0

Table 4.3. The data table for EDS result of 1 second Pt doped SiO_2 thin film.

Element	Weight (%)	Atomic (%)
O	17.74	33.59
Si	55.50	59.85
Sn	24.04	6.14
Pt	2.72	0.42

Table 4.4. The data table for EDS result of 3 seconds Pt doped SiO_2 thin film

Element	Weight (%)	Atomic (%)
O	17.30	32.84
Si	56.07	60.64
Sn	23.75	6.08
Pt	2.88	0.45

Table 4.5. The data table for EDS result of 5 seconds Pt doped SiO_2 thin film.

Element	Weight (%)	Atomic (%)
O	17.30	32.84
Si	56.07	60.64
Sn	23.75	6.08
Pt	2.88	0.58

Also, the porosity is enlarged by increasing the doping concentration of the Pt. These kind of surfaces support the gas sensing. From this, the surface porosity causes the active surface area is increased. On the other hand, the atomic percentage of the Pt which measured from EDS is located in the Table 4.1. It is clearly seen that the atomic concentration of Pt was increased until 0.58% with Pt doping concentration is increase.

4.1.3 Fourier Transform Infrared Spectroscopy (FTIR) Analysis

The identity of the functional groups, molecular interactions, and chemical structure of the tin-oxide thin film which was annealed at 600°C and Pt doped tin-oxide thin films were figured out with Fourier Transform Infrared Spectroscopy (FTIR). The first obtained peak was observed at 530 cm^{-1} from Sn and O non-stoichiometric structure of the tin-oxide (Kaya, 2019). This peak was disappeared after the Pt was doped on the thin film. In XRD analysis section, there was Sn_3O_4

phase, this phase caused the 530 cm^{-1} peak. The peak located at the 591 cm^{-1} comes from the tin-oxide (Peng et al, 2003; Abello et al, 1998).
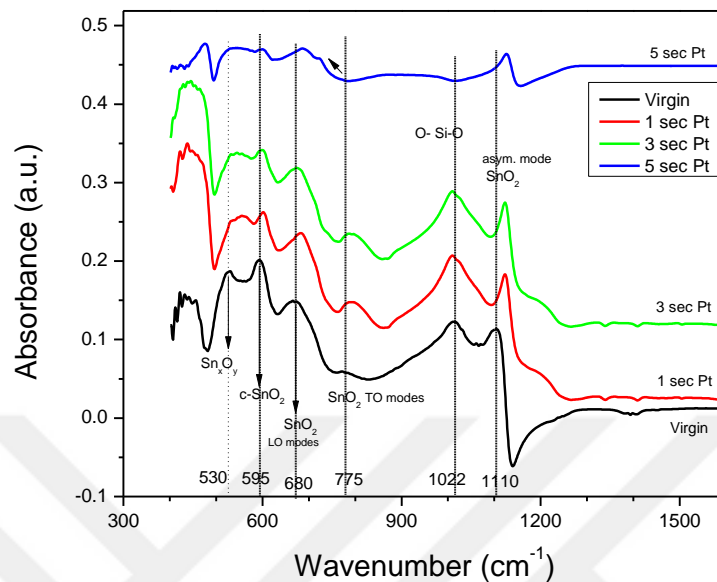
Figure 4.14. The FTIR analysis of the virgin and Pt doped SnO$_2$ thin films.

The intensity of the peak was decreased and slide upward into the high wave numbers thanks to the surface tension. The peaks which are located in 680 cm^{-1} and 775 cm^{-1} along the lines of as against longitudinal and transverse optical modes in tin-oxide bonds (Peng et al, 2003). In longitudinal optic mode the intensity of the tin-oxide is reduced, when the transverse optical mode is increased with Pt doping. These absorption modes of tin-oxide could be related to increasing the expanded vibrations of the tin-oxide bonds in the existence of Pt (Parveen et al, 2018). Rising of the thin film strain and shrinkage of the Pt concentration, they are responsible for longitudinal and transverse optical modes (Peng et al, 2003). In the wave number around 1050 cm^{-1}, the vibrations which are obtained from Silicon-Oxygen-Silicon bonds were decreased and disappeared. Also peak at the wave number at 1110 cm^{-1} is coming from the asymmetric bond vibration of the tin-oxide (Christensen et al, 2016).

With the existence of the stress on the thin film, the peaks were slide, and by Pt doping the band vibration of the tin-oxide was increased. FTIR investigation showed that Pt doping cancels the Sn$_3$O$_4$ phases and catalyzes the tin-oxide phase.

4.1.4 I-V Characterization of the Thin Film

It was observed that, the resistivity were increased with increasing the doping concentration of Pt. According to Sinha et al (2003), doped metals are diffused onto the lattice points of tin-oxide when the vacancies of oxygen are occurs.
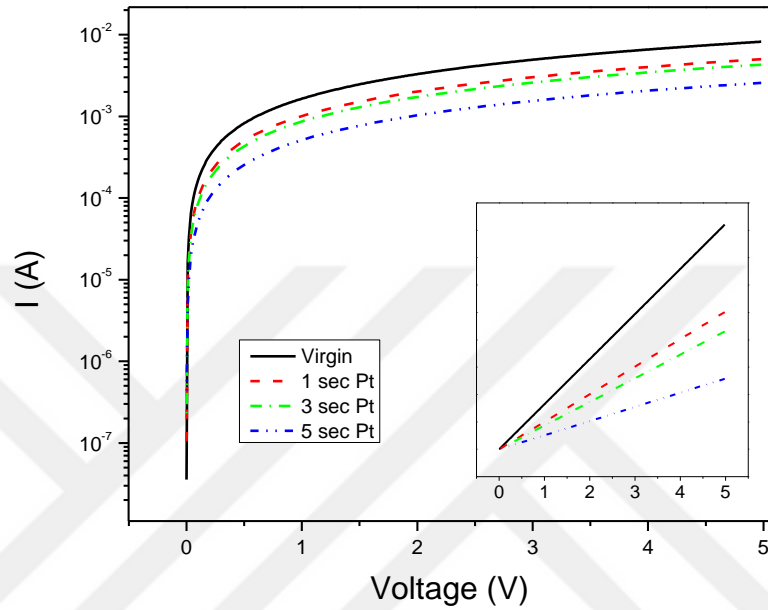
Figure 4.15. I-V characteristics of the tin-oxide thin films in each situation.

Figure 4.15 shows the current-voltage measurements of all thin films; virgin, 1 sec, 3 secs, and 5 secs Pt doped SnO_2 thin films in semi-log scale and linear

4.2 Sensitivity Measurements

After that, the oxygen response of the each materials were measured . The sensor sensitivities (S) of the materials were calculated by Equation 5.3 (Wang et al, 2016).

$$S = \left| \frac{R_{O2} - R_{ref}}{R_{ref}} \right| \qquad (5.3)$$

Where R_{ref} is the resistance of the device in the exposure of N$_2$ gas as initial value, and R_{O_2} is the resistance in the different concentration of O_2.

Figure 4.16. Sensitivities of tin-oxide thin film without Pt deposition and 1 sec, 3 secs, and 5 secs Pt doped thin films at 100°C.

Figure 4.16 shows the graph of the oxygen sensing responses of the tin-oxide based thin film which annealed at 600°C and various amount of Pt doped same thin films. The linear fit was applied on the obtained sensitivities the linear lines on the graph represents the linear fitted lines of the sensitivities of the thin films in under the exposure of different gas concentration at 100°C.

It has been observed that sensitivities of the sensors almost increase with the increasing the Pt concentration and the sensitivity (resistance change) are linearly proportional to O$_2$ concentration. In addition, the higher operation temperature also significantly increases the sensors sensitivities. Types of absorption species and the interaction of target gas with this absorption species are responsible for the observed variations on the sensor sensitivity (Deivasegamani et al, 2017).
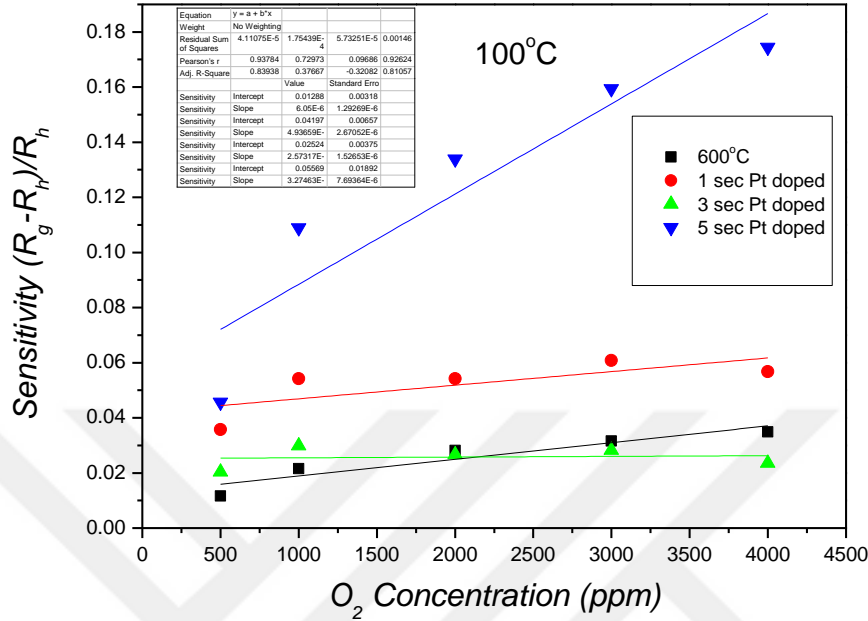
Figure 4.17. Sensitivities of tin-oxide thin film without Pt deposition and 1 sec, 3 secs, and 5 secs Pt doped thin films at 150°C.

Basically there are three types of absorptions species exist including the molecular (O_2^-) and atomic (O^-, O^{2-}) ions depending on the operating temperature (Sun et al, 2012; Deivasegamani et al, 2017; Ghimbeu et al, 2007). It has been reported that below the 150 °C molecular absorption species of the oxygen dominates the sensor response, while above the 150 °C the atomic species are effective on the SnO_2 sensors responses (Sun et al, 2012; Tricoli et al, 2010; Barsan and Wermer, 2001). Hence, sensor sensitivity seen in Figure 4.17 and Figure 4.18 are critically varied with the operation temperatures. These absorption species may capture electrons from the SnO_2. These trapped electrons create a depletion edges resulting in the increase the resistivity of the surface.
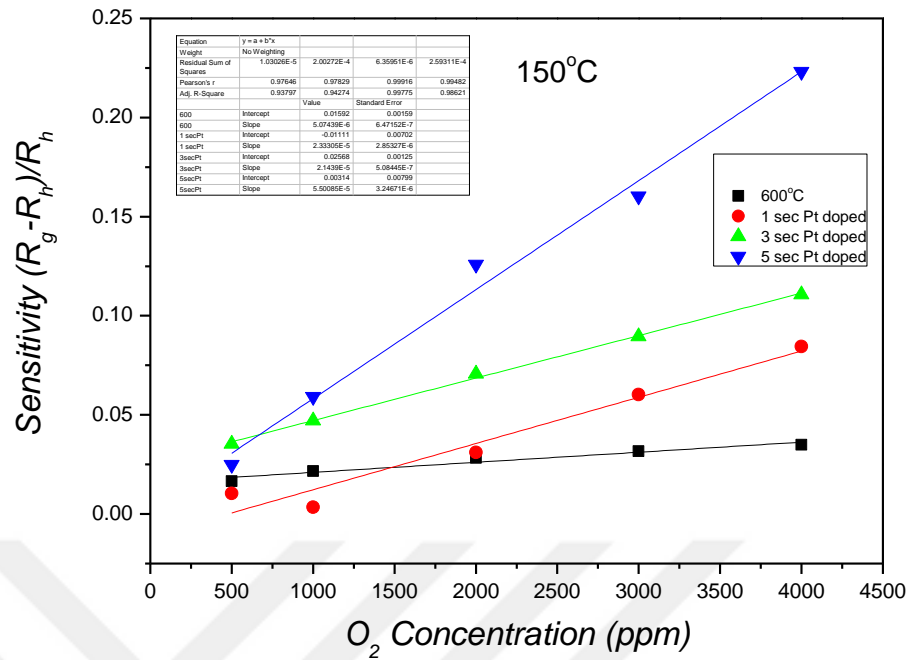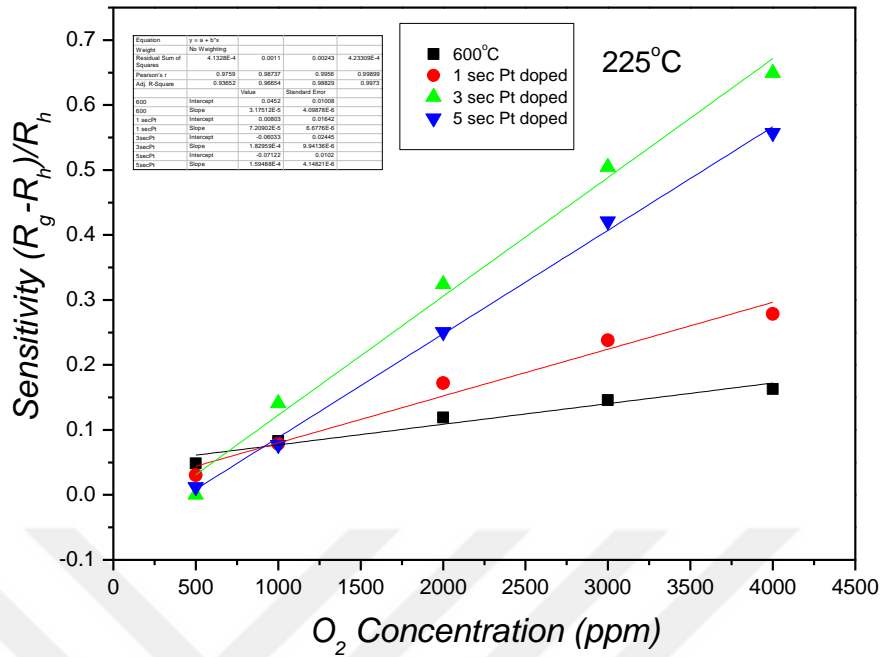
Figure 4.18. Sensitivities of tin-oxide thin film without Pt deposition and 1 sec, 3 secs, and 5 secs Pt doped thin films at 225°C.

On the contrary, in the reference gas environment (N_2 in this study), the trapped electrons by absorption spices returns to SnO_2 lattice which reduces the barrier potential and decrease the resistivity of the surface. Hence, the sensor sensitivities in Figure 4.16, Figure 4.17, and Figure 4.18 increase linearly with increasing the O_2 concentrations. On the other hand, presence of the Pt increases the adsorption activity of the SnO_2. Because the presence of the Pt creates new reaction sites where oxygen molecules can be absorbed in addition to the Sn–O–Sn sites present on virgin SnO_2 (Degler et al, 2016). Hence, the sensor sensitivities increase with the Pt additions.

5. CONCLUSIONS

The SnO_2/SiO_2 thin films were successfully fabricated by the certain methods and annealed at 600^oC. The main object of the study was the investigating the Oxygen response of the device by different doping concentration of Platinum. At the end of the study, it was observed that the Pt doping is definitely effected on the gas sensing property of a metal-oxide semiconductor thin film gas sensors. By increasing the doping concentration, the sensitivity or gas response of the SnO_2/SiO_2 thin films increase in direct proportion. The best results were taken with 5 seconds Pt doped SnO_2/SiO_2 thin films. Also effect of thin film growth and the temperature effect on the gas response of the metal-oxide semiconductor was investigated. In order to device response it was studied at 100^oC, 150^oC, and 225^oC as operating temperature. It is also seen that the temperature is effected the sensitivity of the thin films. 225^oC was the temperature which the best result was obtained in order to sense the oxygen gas in different gas concentration.

6. REFERENCES

Abello L, Bochu B, Gaskov A, Koudryavtseva S, Lucazeau G, Roumyantzeva M (1998) "Structural Characterization of Nanocrystalline SnO$_2$ by X-Ray and Roman Spectroscopy", Journal of Solid State Chemistry, 135: 78-85.

Ahrens LH (1952) "The Use of Ionization Potential Part1. Ionic Radii of the Elements", Geoghimica Acta, 2: 155-169.

Barsan N and Wermer U (2001)" Conduction Model of Metal Oxide Gas Sensors", Journal of Electroceramics, 7: 143-167

Bochenkov VE and Sergeev GB (2010) "Sensitivity, Selectivity, and Stability of Gas-Sensitive Metal-Oxide Nanostructures", American Scientific Publishers, 3: 31-52.

Cakir MC (2014) Investigation of Gas Sensing Application of Metal Oxide Thin Films, MSc Thesis, Hacettepe University, Graduate School of Science and Engineering, Ankara.

Christensen PA, Attidekou PS, Egdell RG, Maneelok S, Manning DAC (2016) "An in Situ FTIR Spectroscopic and Thermogavimetric Analysis Study of the Dehydration and Dihydroxylation of SnO$_2$: The Contribution of the (100), (110), and (111) Facets", Pyhsical Chemistry Chemical Physics, 18: 22990-22998.

Coligne JP and Coligne CA (2002) Physics of Semiconductor Devices, First Edition, Kluwer Academic Publishers, California.

Degler D, Carvalho HWP, Kvashnina K, Grunwalt JD, Weimar U, Barson N (2016) "Structure and Chemistry of Surface Doped Pt: SnO$_2$ Gas Sensing Materials", 6: 28149-28155.

Deivasegamani R, Karunanidhi G, Santhosh C, Gopal T, Achari DS, Neogi A, Nivetha R, Pradeep N, Venkatraman U, Bhatnagar A, Jeong SK, Grace AN (2017) " Chemoresistive sensor for hydrogen using thin films of tin dioxide doped with cerium and palladium" Microchimita Acta, 184: 4765-4773

Dey A (2018) "Semiconductor Metal Oxide Gas Sensors: A Review", Material Science and Engineering B, 229: 206-217.

Eranna G, Joshi BC, Runthala DP, Gupta RP (2004) "Oxide Materials for Development of Integrated Gas Sensors, A Comprehensive Review", Critical Reviews in Solid State Materials Sciences, 29: 3-4.

Fliegel W, Behr G, Werner J, Krabbes G (1994) "Preparation, Development of Microstructure, Electrical and Gas-Sensitive Properties of Pure and Doped SnO_2 powders", Sensors and Actuators B: Chemical, 19: 474-477.

Floyd TL (2005) Electronic Devices Conventional Current Version, Seventh Edition, Pearson Education International, New Jersey.

Ghimbeu CM, Schoonman J, Lumbreras M, Saidat M (2007) " Electrostatic Spray Deposited Zinc Oxide Films for Gas Sensor Applications", Applied Surface Science, 253: 7483-7489

He W, Zhang W, Xie P, Li B, Lv X, Jing C, Liu D "Compositional Correlation and Polymorphism in BaF_2-PrF_3 Thin Films Deposited Using Electron-Beam Evaporation", Thin Solid Films, 669: 558-563.

Kaya S, Yilmaz E, Karacali H, Cetinkaya AO, Aktag A (2015) "Samarium Oxide Thin Films Deposited by Reactive Sputtering: Effects of Sputtering Power and Substrate Temperature on Microstructure, Morphology and Electrical Properties", Material Science in Semiconductor Processing, 33: 42-48.

Kaya S (2019) " Evolutions on Surface Chemistry, Microstructure, Morphology, and Electrical Characteristics of SnO_2/P-Si Heterojunction Under Various Annealing Parameters", Journal of Alloys and Compounds, 778: 889-899.

Korotchenkov G (2007) "Metal Oxides for Solid State Gas Sensors: What Determines Our Choice?", Material Science and Engineering B, 139: 1-23.

Korotchenkov G (2013) Handbook of Gas Sensor Materials Properties, Advantages, and Shortcomings for Applications Volume1: Conventional Approaches, Springer, London

Lee S.P. (2017). Electrodes for Semiconductor Gas Sensors. Sensors (Basel, Switzerland), 17(4), 683. doi:10.3390/s17040683

C.C. Ling, T.C. Guo, W.B. Lu, Y. Xiong, L. Zhu, Q.Z. Xue, Ultrahigh broadband photoresponse of SnO2 nanoparticle thin film/SiO2/p-Si heterojunction. Nanoscale 9, 884.8–8857 (2017).

Matylitskaya VA, Brunkahl O, Kothleitner G, Bock W, Kolbesen BO (2007) "Annealing of Evaporated and Sputtered Niobium Films in Oxygen and Nitrogen Rich Atmospheres by Rapid Thermal Processing (RTP)", Physica Status Solidi C, 6: 1802-1816.

Mishra RK, Sahay PP (2012) "Synthesis, Characterization and Alcohol SensingProperty of Zn-Doped SnO_2 Nanoparticles", Seramics International, 38: 2295-   2304.

Ohring M (1992) Materials Science of Thin Films, Academic Press, New Jersey.

Oyabu T(1982), "Sensing Characteristics of SnO2 Thin Film Gas Sensors", Journal of Applied Physics, 53: 2785-2787

Oztel O (2018) IV-VI Grubu Bileşiklerin Nanoboyutta Üretimi ve Optik Özelliklerinin İncelenmesi, MSc Thesis, İstanbul University, Fen Bilimleri Enstitüsü, İstanbul.

Parveen A, Agrawal S, Azam A (2018) "Band Gap Tunning and Fluorescence Properties of Lead Sulfide $Pb_{0.9}A_{0.1}S$ (A: Fe, Co, and Ni) Nanoparticles by Transition Metal Doping", Optical Materials, 76: 21-27.

Peng XS, Zhang LD, Meng GW, Tian YT, Lin Y, Geng BY, Sun SH (2003) "Micro-Roman and Infrared Properties of SnO_2 Nanobelts Synthesized From Sn and SnO_2 Powders", Journal of Applied Physics, 93: 1760-1763.

Poole CP, Owens FJ (2003) Introduction to Nanotechnology, John Wiley and Sons Inc, New Jersey.

Sardela M (2014) Practical Materials Characterization, Springer, New York

Scherrer P (1918) "Bestimmung der Grösse, und der inneren Struktur von Kolloidteilchen mittels Röntgenstrahlen, Nachrichten von Der Gesellschaft Der Wissenschaften Zu" Göttingen, Math. Kl. 1918 98–100, http://dx.doi.org/10.1007/978-3-66233915-2.

Sinha SK, Ray SK, Manna I (2014) "Effect of Al Doping on Structural, Optical and Electrical Properties of SnO_2 Thin Films Synthesized by Pulsed Laser Deposition", Philosophical Magazine, 94: 3507-3521.

Sun YF, Liu SB, Meng FL, Liu JY, Jin Z, Kong LT, Liu JH (2012) " Metal Oxide Nanostructures and Their Gas Sensing Properties: A Review", Sensors-Basel, 12: 2610-2631

Tangriala VKK, Pozos HG, Lugo VR, Olvera ML (2017) "A Study of the CO Sensing Responses of CU-Pt-and-Pd-Activated SnO_2 Sensors: Effect of Precipitation Agents, Dopants and Doping Methods", Sensors, 17: 2-24.

Tricoli A, Righettonni N, Teleki A (2010) "Semiconductor Gas Sensors: Dry Synthesis and Application" Angew Chem. Int. Ed. Engl., 49: 7632-7659

Wang C, Yin L, Zhang L, Xiang D, Gao R, (2010) "Metal Oxide Gas Sensors: Sensitivity and Influencing Factors", Sensors, 10: 2088-2106.

Wang T, Huang D, Yang Z, Xu S, He G, Li X, Hu N, Yin G, He D, Zhang L (2016) "Areview on Graphene Based Gas/Vapor Sensors with Unique Properties and Potential Applications", Nano-Micro Letters, 8:95-119

Yamazoe N (2005) "Toward Innovation of Gas Sensor Technology", Sensors and Actuators B, 108:2-14.

Zhang G and Liu M (2000) " Effect of particle size and dopant on properties of SnO$_2$- based gas sensors" Sensors and Actuators B, 69: 144-152.

7. CIRRUCULUM VITAE

Name SURNAME   :Sinan Öztel

Place and Date of Birth   : Of/1988

Universities

Bachelor's Degree   : Abant İzzet Baysal University, Physics

e-mail   : oztelsinan@gmail.com

Address   : Hasanpaşa Mah. Kurbağalıdere Cad.
                         Abdulhalim Memduh Sk. No: 4/2
                         Kadıköy/İSTANBUL

List of Publications   :

- **Oztel S**, Kaya S, Budak E, Yilmaz E (2019) "Influences of platinum doping concentrations and operation temperatures on oxygen sensitivity of Pt/SnO2/Pt resistive gas sensors" Journal of Materials Science: Materials in Electronics, https://doi.org/10.1007/s10854-019-01854-4